

Remotely sensed carbon content: The role of tree composition and tree diversity



Christine I.B. Wallis^{a,*}, Anna L. Crofts^a, Deep Inamdar^b, J. Pablo Arroyo-Mora^c, Margaret Kalacska^b, Étienne Laliberté^d, Mark Vellend^a

^a Département de biologie, Université de Sherbrooke, Sherbrooke, QC, Canada

^b Applied Remote Sensing Lab, Department of Geography, McGill University, Montréal, QC, Canada

^c National Research Council of Canada, Flight Research Lab, Ottawa, ON, Canada

^d Institut de recherche en biologie végétale, Département de sciences biologiques, Université de Montréal, Montréal, QC, Canada

ARTICLE INFO

Edited by Dr. Marie Weiss

Keywords:

Aboveground biomass
Hyperspectral reflectance
Spectral diversity
Carbon storage
Functional leaf traits
Functional dispersion
Functional composition
Leaf economics spectrum
Mass ratio hypothesis
Phylogenetic composition
Phylogenetic diversity

ABSTRACT

Optical remote sensing permits modeling of variables related to forest biomass, which is a critical determinant of carbon (C) stocks and fluxes. Plant functional characteristics can be captured by (hyper)spectral data, but it remains unclear whether the links between spectral information and C content are driven largely by tree composition, tree diversity, or by forest attributes not commonly measured in field inventories (e.g., physical canopy structure). Here, we examine the relationship between hyperspectral reflectance and aboveground C content in forests, testing the relative importance of tree composition and diversity in mediating this relationship. We use hyperspectral imaging data from an airborne survey with precisely geo-located field data on canopy trees in two forests in southern Québec, Canada. Spectral data covering visible (VIS), near infrared (NIR) and short-wave infrared (SWIR) wavelengths were extracted for 2626 tree crowns within 64 field plots distributed along an elevational gradient. We applied a continuum removal to the spectra and subsequently performed a principal component analysis to reduce the spectral dimensionality. From the spectral principal components, for each plot we quantified (i) spectral composition (based on average reflectance per plot), and (ii) spectral diversity using the convex hull volume. From field data, we calculated variables characterizing the taxonomic, functional and phylogenetic composition and diversity of canopy trees. Carbon content was calculated using allometric equations based on tree size. We applied a structural equation model based on partial-least squares to test both indirect effects of spectral composition and diversity on C storage of trees (via on-the-ground tree composition or diversity), and also direct effects (reflecting forest characteristics unmeasured in field surveys). We found that spectral composition, particularly from the VIS, is related to C content largely indirectly, via changes in tree composition along the elevational gradient (a transition from deciduous to coniferous species with increasing elevation). Though spectral diversity was significantly related to tree species diversity, no direct or indirect effects on C content were detected. Overall, our findings support (i) the importance of tree composition (but not diversity) in mediating the link between hyperspectral data and forest C content, and (ii) the use of hyperspectral remote sensing as an effective surrogate of taxonomic, functional, and phylogenetic composition of tree communities with strong links to C storage.

1. Introduction

Tree biomass is a key parameter in models of the global carbon cycle (Houghton et al., 2009). As such, there is a need for spatially explicit estimates of carbon stocks and fluxes in forests, especially given their use in land use management aimed at mitigating rising carbon emissions. Forest carbon (C) content is effectively an ecosystem service.

Standardized monitoring of large forest areas is time- and labor-intensive, but it can be supported by remote sensing surrogates (Xiao et al., 2019). Optical remote sensing (i.e., passive detection of spectral reflectance) from air and space and at different spatial and spectral resolutions has proven to successfully predict tree aboveground biomass (AGB) and C content (which is approximately 50% of tree AGB; Xiao et al., 2019). This is particularly the case when light detection and

* Corresponding author.

E-mail address: christine.wallis@USherbrooke.ca (C.I.B. Wallis).

ranging (lidar) data are not available (Naik et al., 2021; Wallis et al., 2019) or as complementary predictors (Almeida et al., 2021; Castillo et al., 2017; Li et al., 2020; Puliti et al., 2020). However, it is not fully understood which canopy tree properties are captured by optical sensors when predicting C content. Understanding this relationship could greatly improve the ecological interpretation of C content estimates derived from spectral reflectance.

From an ecological perspective, plant composition (e.g., trait values of dominant species) or plant diversity, are thought to be important factors influencing ecosystem functions such as C content. The mass ratio hypothesis (Grime, 1998) refers to the effects of plant composition in terms of functional traits (Xu et al., 2020; Yuan et al., 2018), which include the morphological, physiological, and phenological characteristics of plant leaves (or other parts) that have direct effects on their growth, reproduction and survival (Violle et al., 2007). At the community-level, mean functional traits (across species) are considered to be integrative indices of plant resource requirements and usage (Cadotte, 2017). Many plant traits are intercorrelated, with the leaf economics spectrum (LES) characterizing a tradeoff between resource acquisition (e.g., thin, high-nitrogen, short-lived leaves with rapid photosynthesis) and storage (the opposite characteristics), with major impacts on ecosystem functions (Reich, 2012, 2014; Wright et al., 2004). For instance, Reich (2012) found that canopy nitrogen (N) concentrations and leaf area index explain >75% of the variation in net primary production of temperate and boreal forests.

The niche complementary hypothesis, in contrast, suggests that higher plant diversity (implying variable resource use strategies) leads to more efficient resource acquisition and thus increased ecosystem functions (Tilman et al., 1997). Compared to taxonomic diversity, functional and phylogenetic diversity tend to have stronger links to ecosystem functions (Cadotte et al., 2009, 2011). Both the mass ratio and niche complementarity hypotheses have been intensively discussed within ecology, and with regard to forest AGB or C content, evidence can be found for both (Finegan et al., 2015; Paquette and Messier, 2011; Rawat et al., 2019; Ruiz-Benito et al., 2014). As such, both tree composition and tree diversity have the potential to provide a link between forest C storage and remotely sensed forest characteristics.

While multispectral sensors can detect large differences in canopy properties, the narrow wavelength bands of hyperspectral remote sensing provide greater potential for estimating functional leaf and canopy traits (Serbin and Townsend, 2020). Several studies have used hyperspectral imaging data to address tree composition (i.e., community weighted mean traits; Homolová et al., 2013), tree diversity (Wang and Gamon, 2019), biomass (Williams et al., 2021) and related ecosystem functions such as productivity (Smith et al., 2002). For example, airborne hyperspectral data have been used to successfully model and map traits related to the leaf economics spectrum in tropical ecosystems (e.g., Asner et al., 2016) as well as sub-boreal and temperate forests (e.g., Singh et al., 2015). Remote sensing has also addressed taxonomic and phylogenetic composition, which are typically quantified using synthetic ordination axes derived from analyses of plot-to-plot pairwise dissimilarity matrices (Feilhauer and Schmidlein, 2009; Rocchini et al., 2018; Wallis et al., 2017).

Multiple dimensions of plant diversity have also been estimated based on spectral diversity metrics (Wang and Gamon, 2019). The spectral variation hypothesis (SVH; Palmer et al., 2002) suggests that a diverse plant community leads to a higher spectral diversity due to higher foliar trait diversity and phylogenetically-conserved trait variation among taxa (Carlson et al., 2007; Cavender-Bares et al., 2016). The majority of spectral diversity studies focus on grasslands, with most studies from forests in tropical regions and addressing taxonomic diversity; these studies indicate moderate to high predictive performance (Carlson et al., 2007; Féret and Asner, 2014; Jucker et al., 2018). Schweiger and Laliberté (2022) modeled plant taxonomic and phylogenetic diversity across multiple biomes with varying success; predictions within high-LAI ecosystems such as temperate forests were

more accurate than in low-LAI ecosystems.

A few studies in grasslands (e.g., Schweiger et al., 2018) and forests (Almeida et al., 2021; Jucker et al., 2018; Smith et al., 2002) have estimated ecosystem functions directly from hyperspectral imaging data, under the assumption of an indirect link via plant composition or diversity. Almeida et al. (2021) used lidar and hyperspectral data together, showing that spectral variation is positively linked to tropical tree diversity and AGB. However, studies to date have not been designed to identify indirect relationships in natural environments while considering multiple dimensions of tree composition and diversity at the same time. More explicit tests of indirect relationships can be obtained using structural equation modeling (SEM, also called path modeling), which involves a series of multiple regressions in which intermediate variables, so-called mediators, can be included (Fan et al., 2016). Such analyses can be used to test effects of independent variables both via a direct path to a response variable, or via indirect paths involving mediator variables (Cepeda-Carrion et al., 2018). This can help to identify whether hyperspectral data captures tree compositional or tree diversity metrics when predicting ecosystem functions.

Here, we analyze hyperspectral remote sensing data, C content, and field-based data on canopy trees (taxonomic, functional, and phylogenetic dimensions) within 64 plots in two forests of southern Quebec, Canada. We propose that spectral composition (the average reflectance per plot) and spectral diversity (the variation in spectral reflectance per plot) are potential predictors of C content, and we aim to identify the degree to which these relationships are influenced by tree composition, tree diversity, or unmeasured aspects of forest canopies. For this purpose, we use a SEM to disentangle indirect links (mediated by tree composition and diversity) from spectral composition and spectral diversity to aboveground C storage, as well as direct links (suggestive of unmeasured canopy characteristics). We additionally include data on topography to account for changes along the elevational gradient. Our goal is to enhance the ecological understanding of remotely sensed ecosystem functions such as C content in forests and its implications for future studies.

2. Methods

2.1. Study area

This study was conducted at two forest sites in southern Quebec, Canada: Parc national du Mont Mégantic (hereafter, Mont Mégantic) and Parc national du Mont-Saint-Bruno (hereafter, Mont-Saint-Bruno; Fig. 1 a, b). Mont Mégantic is situated in the Northern Appalachian Mountain region and spans an elevational gradient (430 to 1105 m a.s.l.), where the forest transitions from the deciduous dominated, northern temperate forest to coniferous dominated, boreal forest with increasing elevation. Lower elevations are dominated by *Acer saccharum* (sugar maple), *Betula alleghaniensis* (yellow birch), and *Fagus grandifolia* (American beech), mid elevations by *B. alleghaniensis*, *Abies balsamea* (balsam fir), *Picea rubens* (red spruce) and *Betula papyrifera* (paper birch), and high elevations by *A. balsamea*, *B. papyrifera* and *Sorbus spp.* (Mountain ash). This change in tree species composition is driven by changes in climatic conditions, where mean annual temperature is ~4 °C at low elevations and declines by 0.64 °C every 100 m increase in elevation (Parc national du Mont Mégantic (PNMM), 2007). In addition to changes in climate, soil properties change along the elevational gradient and may also affect tree species composition and diversity (Carteron et al., 2020). A more detailed synthesis of the tree composition at Mont Mégantic, in particular under changing climatic conditions, can be found in Vellend et al. (2021).

Mont-Saint-Bruno is located 170 km west of Mont Mégantic in the Saint Lawrence Lowland region; elevation ranges from 30 to 208 m a.s.l. The climate is warmer than at Mont Mégantic, with a mean annual temperature of 6 °C (Environment and Climate Change Canada, 2011). The forest is predominantly deciduous, northern temperate forest where

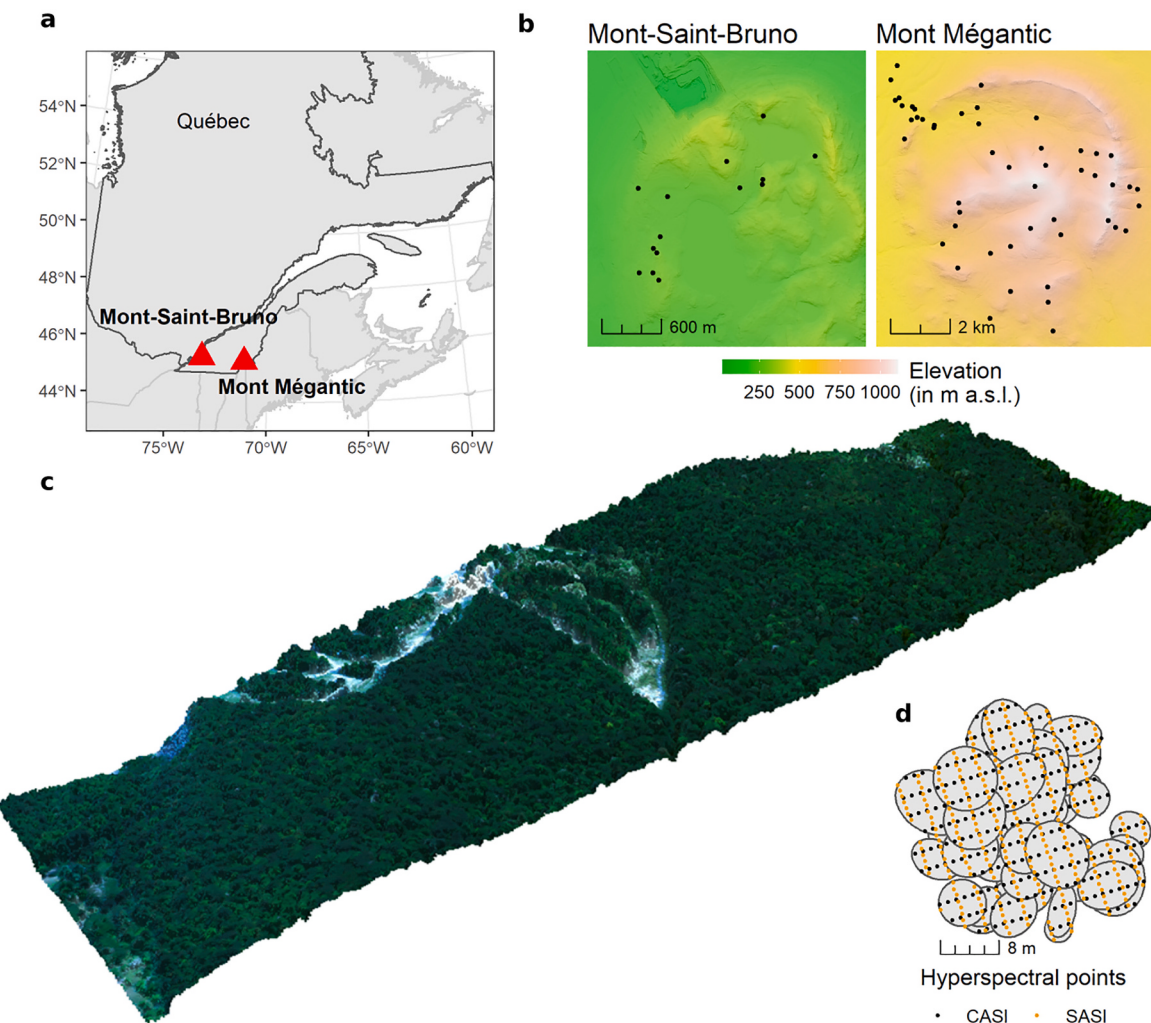


Fig. 1. Location of the study area within southern Quebec, Canada (a). Elevation (provincial lidar data, 1 m spatial resolution) and field plot positions (black dots) at Mont-Saint-Bruno and Mont Mégantic (b). Exemplary RGB presentation of the hyperspectral point cloud (DHPC; Inamdar et al., 2021a, 2021b) after continuum removal at Mont-Saint-Bruno (c) and the DHPC of the two sensors and the delineated visible canopy at one of the forest plots at Mont Mégantic (d).

the dominant species are similar to those in the low elevation stands at Mont Mégantic but include additional southerly, “thermophilic” species such as *Carya cordiformis* (bitternut hickory) and *Ostrya virginiana* (American hop-hornbeam) at the northernmost limits of their ranges.

2.2. Data

2.2.1. Field sampling of tree properties, functional traits, above-ground biomass and C content

Forest inventories were conducted in the summers of 2019 and 2020 within 64 plots: 50 plots at Mont Mégantic and 14 plots at Mont-Saint-Bruno. Dimensions of all plots have been corrected for slope in the field, resulting in circular plots of 15 m radii as viewed from above, covering an area of approximately 706 m². Plot centers were positioned using a high-accuracy GPS method (Trimble Catalyst DA1 antenna with GNSS service, Trimble Inc.; Crofts et al., 2022). Whenever possible, Trimble RTX corrections delivered via the Internet and otherwise via satellites (when out of cell service) were used to achieve high position accuracy (mean horizontal accuracy of 0.2 m; Crofts et al., 2022).

Within each plot, we surveyed all trees with crowns that extended into the upper canopy and any trees with crowns completely below the upper canopy but with a diameter at breast height (dbh) >9 cm. The sampling protocol for the positioning of the trees and the sampling of tree parameters are detailed in Crofts et al. (2022). Briefly, each tree was

identified to species, measured for dbh and height, and assigned a crown class (i.e., a categorical variable that describes vertical position and dominance of crowns defined by NRCan, 2008). Tree height (distance between the base of the tree and the tip of the highest branch) was measured using a range finder with integrated tilt sensor (LaserGeo). A suite of crown measurements, including spatial position, maximum length and orthogonal width, were measured in order to model crowns as ellipses, from which we estimated their areas (see supplementary data).

We expect the spectral diversity-plant diversity relationship to be strongest when only the crown portions exposed to direct overhead light are used (Carlson et al., 2007; Schweiger and Laliberté, 2022). In a GIS-based approach in R (Core and Team, 2020), we therefore subsetted the field-based data to retain only information on the visible canopy (i.e., the uppermost layer of the canopy) using the ‘sf’ package (Pebesma, 2018). To do so, we determined the vertical order of overlapping crowns by first filtering crowns based on their assigned crown class and then, by tree height. Subsequently, we cut the overlapping crowns according to their vertical order and retained crown segments that had no overhead obstructions (i.e., visible from above; Fig. 1 d). Relative species abundance was calculated as the plot-wise proportional area of all retained crown segments per species. Going forward, this relative species' abundance was used to weight plot-wise composition and diversity measurements.

Leaf sampling and trait measurements followed the standardized protocols developed by the Canadian Airborne Biodiversity Observatory (CABO; [Ayotte and Laliberté, 2019](#); [Crofts and St-Jean, 2022](#); [Girard et al., 2021](#); [Laliberté, 2018](#)). For the most abundant tree species, leaves were sampled from 10 or more individuals; for less common tree species ($n = 6$; see [Crofts et al., 2022](#) for a list of all observed tree species) leaves were sampled from five or more individuals (see sampling protocol in [Crofts and St-Jean, 2022](#)). For one species (*Alnus incana*) leaves from only three individuals were sampled. For each individual, a twig from the upper canopy (>3 h of estimated direct daily sunlight) was collected with at least 6 mature and healthy leaves (or arrays of leaves in the case of small leaves and coniferous species). In total, we used 14 foliar traits, covering structural and chemical leaf traits, pigments, and carbon fractions (Appendix A Table A1). Leaf trait values were pooled from both sites and we calculated the community-weighted mean (CWM) trait values per plot, where the mean trait values were weighted by species abundance.

We calculated tree AGB for each plot based on allometric equations using dbh, tree height, and model parameters from Canadian forest ecosystems published in [Lambert et al. \(2005\)](#). As parameters were not available for certain tree species, we followed the approach in [Crockett et al. \(2021\)](#) and used the parameters of the closest phylogenetic relatives determined from [Qian and Jin \(2016\)](#); in the case of multiple equally related species (i.e., unresolved clusters of >2 close relatives), we used the averaged parameters from these species. Tree AGB was further converted to the mass of aboveground carbon (C content) using species-specific carbon-biomass relationships from [Lamlom and Savidge \(2003\)](#). For species without published C content in relation to AGB, we again identified the phylogenetically closest relative(s) and used their published relationship(s). Plot-level statistics such as average dbh, tree height, crown area, AGB, C content, and tree type as well as species dominance can be found in the supplementary data.

2.2.2. Tree composition, tree diversity and topography measures

Our study aimed to compare the effects of the multidimensional concepts of tree composition and tree diversity in mediating the relationship between hyperspectral reflectance and C content. Therefore, we characterized these two concepts considering taxonomic, functional and phylogenetic dimensions. Tree composition was characterized by first analyzing the change in species identity across plots using dissimilarity matrices (also known as beta diversity); ordination techniques were then applied to derive numerical scores on synthetic compositional axes for each field plot (see e.g., [Feilhauer and Schmidlein, 2009](#); [Rocchini et al., 2018](#); [Wallis et al., 2017](#)). For all tree species composition and diversity variables, we used the plot-wise crown areas of species as a measure of abundance.

Functional composition was based on a principal component analysis (PCA) using all 14 CWM trait values. Taxonomic and phylogenetic composition, in contrast, are based on non-Euclidean distances (which are not affected by the number of null values between samples), which we subjected to non-metric multidimensional scaling (NMDS) ordinations, which can handle any dissimilarity matrix and any user-defined number of dimensions. For the taxonomic dimension, we calculated pairwise Bray-Curtis dissimilarities based on species abundances between all plots. Subsequently, we performed NMDS using the R function metaMDS in ‘vegan’ ([Oksanen et al., 2020](#)). We used the site scores of the dimensions as proxies for tree species’ composition. For phylogenetic composition, we used a phylogenetic tree derived from the phylocom software ([Webb et al., 2008](#); [Webb and Donoghue, 2005](#)). We again used NMDS to perform dimension reduction based on phylogenetic dissimilarities (i.e., cophenetic distances) calculated between each pair of plots using the R package ‘picante’ ([Kembel et al., 2010, 2020](#); [Webb et al., 2008](#)) and ‘ape’ ([Paradis and Schliep, 2019](#)). We chose two dimensions for the taxonomic and phylogenetic NMDSs, which both had stress values <0.2, indicating appropriate NMDS solutions.

When calculating tree diversity, we also considered all three

dimensions. To quantify taxonomic diversity, we calculated the Shannon-Wiener index in the ‘vegan’ package in R ([Oksanen et al., 2020](#)). Based on all 14 CWM trait values, we calculated functional diversity using the ‘FD’ package in R ([Laliberté et al., 2014](#); [Laliberté and Legendre, 2010](#)). We chose functional dispersion (FDIs) which can be weighted by species abundance and can also handle communities with a single tree species. For phylogenetic diversity, we used the mean-pairwise distances (MPD) calculated in the R package ‘picante’ ([Kembel et al., 2020](#)).

To account for topographical changes across all plots that might affect tree species composition, diversity, and C content, and that likely correlate with changes in climate and soil, we derived elevation and slope from lidar data (spatial resolution of 1 m) acquired by the Quebec provincial government ([Leboeuf et al., 2015](#)) and calculated northness based on aspect, and the topographic position index (TPI) using the R package ‘terra’ ([Hijmans et al., 2021](#)).

2.2.3. Hyperspectral remote sensing data and spectral diversity

An airborne hyperspectral survey was conducted on 18/07/2019 at Mont Mégantic and on 08/09/2018 at Mont-Saint-Bruno by the National Research Council of Canada, Flight Research Lab (NRC-FRL). Two sensors were on-board the NRC-FRL’s Twin Otter fixed-wing aircraft, the Compact Airborne Spectrographic Imager (CASI-1500) and the Short-wave infrared Airborne Spectrographic Imager (SASI). The CASI-1500 is a pushbroom imager that collects spectral information over 288 spectral bands (375–1061 nm) and 1498 effective spatial pixels that span the sensor’s 39.8° field of view. The SASI is a pushbroom imager with two optical trains that collects spectral information over 100 spectral bands (957–2442 nm) and a total of 600 effective spatial pixels that span the sensor’s 39.7° field of view. The raw hyperspectral data collected underwent standard pre-processing steps including a radiometric and atmospheric correction, as well as a geometric and statistical-empirical BRDF topographical correction using the digital surface model from the provincial lidar mission ([Inamdar et al., 2021a](#)).

In conventional hyperspectral imaging data processing procedures, the output of the geometrically corrected data is spatially resampled on a uniform grid using a nearest neighbor approach to generate a square pixel raster data structure. This spatial resampling process compromises data integrity as pixels from the original hyperspectral imaging data are shifted, duplicated or eliminated to fit the raster data model. For example, when using raster end products in areas with large elevational gradients, the choice of a constant spatial resolution is often a compromise between down sampling (pixel loss) and upscaling (pixel duplication) since the spacing of spectral measurements differs between higher and lower elevations. As the spectral values can shift spatially in square pixel raster formats, the potential raster end product will have resampling errors on top of positioning errors. Instead of the common georeferenced raster format, here we used a new data format of hyperspectral imaging data, the directly-georeferenced hyperspectral point cloud (DHPC; Fig. 1 c; [Inamdar et al., 2021a, 2021b](#)). By avoiding the spatial resampling step in conventional processing procedures, the DHPC preserves the spectral-spatial integrity of the imaging data without shifts, loss or duplication of spectral measurements. Recent work using DHPCs suggests a higher precision of the location of a spectral measurement, which is particularly of value for airborne hyperspectral imaging across elevational gradients ([Inamdar et al., 2021a](#)) and for applications at the scale of individual tree crowns. The spatial resolution of the CASI and SASI DHPCs from Mont Mégantic were ~2.4 and ~2.7 m, respectively. The spatial resolution of the CASI and SASI DHPCs from Mont-Saint-Bruno were ~1.7 m and ~1.8 m, respectively (see Appendix Table A2 for more detail).

All spectral points were projected to UTM 19 North for plots at Mont Mégantic and UTM 18 North for plots at Mont-Saint-Bruno, respectively. We used a red band (679.11 nm) to filter shadowed areas using a threshold of 75 (reflectance *10000) based on visually identified cloud and canopy shadows. Non-forest-areas were excluded based on a NDVI

filter ($\text{NDVI} < 0.75$; inferred from statistics of training sites and visual interpretation at both sites). Since the two sensors were not spatially aligned, we averaged the CASI and SASI spectra per individual tree crown visible from above and extracted only those spectra for which there was a signal from both sensors. This procedure reduced the number of studied tree crowns but allowed for the use of the full spectrum of hyperspectral wavelengths. The resulting averaged spectra per individual tree crown or crown fragment rely on the spatial matching of crowns delineated in the field and hyperspectral points. Although field data as well as airborne spectra were measured using very precise geo-location systems, they both include a positioning error. We therefore removed small crown fragments ($< 2\text{m}^2$) which are likely to include overlapping crowns and where we assume a higher matching error of crown shape and spectral measurement. The spectra of the two sensors at each of the remaining 2626 tree crowns were matched using the package ‘spectrolab’ (Meireles et al., 2017). As in Osei Darko et al. (2021), we excluded the low signal and noisy regions ($< 450 \text{ nm}$ and $> 900 \text{ nm}$ for CASI and $> 2430 \text{ nm}$ for SASI) as well as the water absorption regions within the SWIR bands, which showed significant noise (1345 nm–1460 nm and 1790 nm–1950 nm). We recognize that water absorption regions can provide important information for plant trait retrieval (Curran, 1989), but prioritization of these bands was not the focus of our analysis. We further applied the Savitzky-Golay smoothing filter within a defined window size of 21 bands and a polynomial of 4th order. Finally, we applied a continuum removal using the convex hull band depth ratio in the package ‘hsdar’ to further normalize reflectance data from the different flightlines (Lehnert et al., 2019).

We applied a PCA to reduce the dimensionality of continuum-removed reflectance of the remaining 267 bands for each tree crown individual. As measures of spectral composition, we investigated all spectral principal components (PCs) that explained $> 1\%$ of the variance, and averaged them per plot using their weighted means by crown size. Several spectral diversity metrics have been investigated ranging from the band-wise coefficient of variation (Wang et al., 2017) to spectral variance, which can be used to partition spectral diversity into alpha and beta diversity components (Laliberté et al., 2020; for a comprehensive overview of most spectral diversity metrics see the supplementary data in Frye et al., 2021). Some of the investigated spectral diversity metrics are mathematically very similar or identical to ecological metrics such as the convex hull volume (CHV, defined as the volume of the first three principal components of spectral data; Dahlin, 2016; Gholizadeh et al., 2018), a metric also used for functional trait diversity (Cornwell et al., 2006). For these reasons, we calculated the CHV of the first three principal components for each plot to quantify spectral diversity as described in Cornwell et al. (2006) and Dahlin (2016). We used the log-transformed CHV values to address skewness.

2.3. Methods

2.3.1. SEM-PLS: Direct and indirect effects in modeling C content

SEMs based on partial least squares (SEM-PLS) aim to identify direct and indirect relationships between blocks of indicators (also called manifest vectors) represented by constructs (also called latent vectors; Benitez et al., 2020). Though SEM-PLS is rarely used in remote sensing studies (but see Lopatin et al., 2019), it is well suited to relatively small sample sizes, and can combine multiple variables into single constructs, which is often appropriate when combining multiple, high-dimensional constructs such as those derived from hyperspectral and field-based inventories.

Based on the niche complementary and the mass ratio hypotheses, we propose that spectral composition (the average reflectance per plot) and spectral diversity are potential predictors of C content and further that their relationships are mediated by tree composition and tree diversity, respectively. Since we seek to better understand the relationship between spectral reflectance and C content, and which on-the-ground tree properties are captured when estimating C content from

hyperspectral reflectance, we here used the SEM-PLS in an exploratory way and not in its original hierarchical-cause way (i.e., we do not analyze causal effects from tree composition/diversity to reflectance). We use the SEM-PLS to identify the indirect and direct relationships of spectral composition, spectral diversity, and topography with above-ground C content in trees (hereafter referred to as C content), considering the two mediators tree composition and tree diversity (Fig. 2). In the inner model, constructs are connected to each other through path coefficients and in the outer model, indicator variables are connected with their construct through weights (Hair et al., 2021a). The weights in the outer model are defined as either reflective or formative (Tenenhaus et al., 2005). For instance, tree composition was measured using a formative mode, i.e., the indicator weights are based on multiple regressions assuming that the axes of taxonomic, functional and phylogenetic turnover do not necessarily share the same theme (e.g., multiple environmental gradients), and therefore, they are ideally not correlated. For tree diversity, in contrast, we chose a reflective mode since we assume that taxonomic, functional and phylogenetic tree diversity share the same theme and are correlated.

After the initial model is set up, SEM-PLS maximizes the coefficient of determination (r^2) values of tree composition/diversity as well as C content by iteratively changing the weights of indicator variables; this procedure is repeated until the path coefficients stabilize (Hair et al., 2021a; Lohmöller, 2013). SEM-PLS is validated and adjusted by multiple criteria including the removal of variables in the outer model due to high pairwise correlations (e.g., for tree composition) or the insignificance of weights. A full report for all criteria can be found in the supplementary data. Bootstrapping using 10,000 sample data sets was used to derive t-values at the 1% level for the indicator weights and loadings as well as confidence intervals for the path coefficients in the inner model. The pathways of the inner model are evaluated by comparing the strength and significance of the direct and indirect paths. Mediation exists if the predictor construct (i.e., spectral composition, diversity or topography) is related to the mediator (i.e., tree composition or diversity) that in turn affects the endogenous construct (C content). To assess the explanatory power for C content as well as for tree composition and tree diversity, r^2 values are used. Moreover, we assessed the predictive power of the path model in estimating C content. For this purpose, we removed all insignificant paths to C content and applied a 10-fold cross validation and compared the derived root mean square error (RMSE) values with those derived from a 10-fold cross-validated linear regression model using the indicator variables of all remaining constructs. A high predictive power of the path model is achieved if its RMSE values are lower compared to that of the linear model (Shmueli et al., 2019). All model analyses and validation has been performed using the R package ‘seminR’ (Hair et al., 2021b).

3. Results

3.1. Indicator selection and relevance within constructs

For the construct spectral composition, we identified three significant spectral axes (Fig. 3 a), with the highest contribution from spectral axis 1 ($w = 0.75, p < 0.01$), followed by spectral axis 5 ($w = -0.48, p < 0.1$), and spectral axis 3 ($w = 0.31, p < 0.01$). The first spectral axis showed high negative scores in the visible region; the fifth spectral axis showed contributions from multiple absorption features in the VIS, NIR and SWIR regions, and the third axis showed high positive scores in the blue and negative scores in the SWIR region around 2000 nm (Fig. 4 a).

Tree composition was mostly determined by taxonomic axis 1 ($w = 0.97, p < 0.001$, Fig. 3 a), identifying a turnover in tree species composition (Fig. 4 c) that was correlated to the percentage of coniferous cover per plot ($r = 0.89, p < 0.001$; Appendix A Fig. A1). Functional and phylogenetic turnover along the first axes have been removed due to high correlations with the taxonomic axis 1 ($r > 0.85, p < 0.001$; Appendix A Fig. A1); these correlations indicate coupled changes in

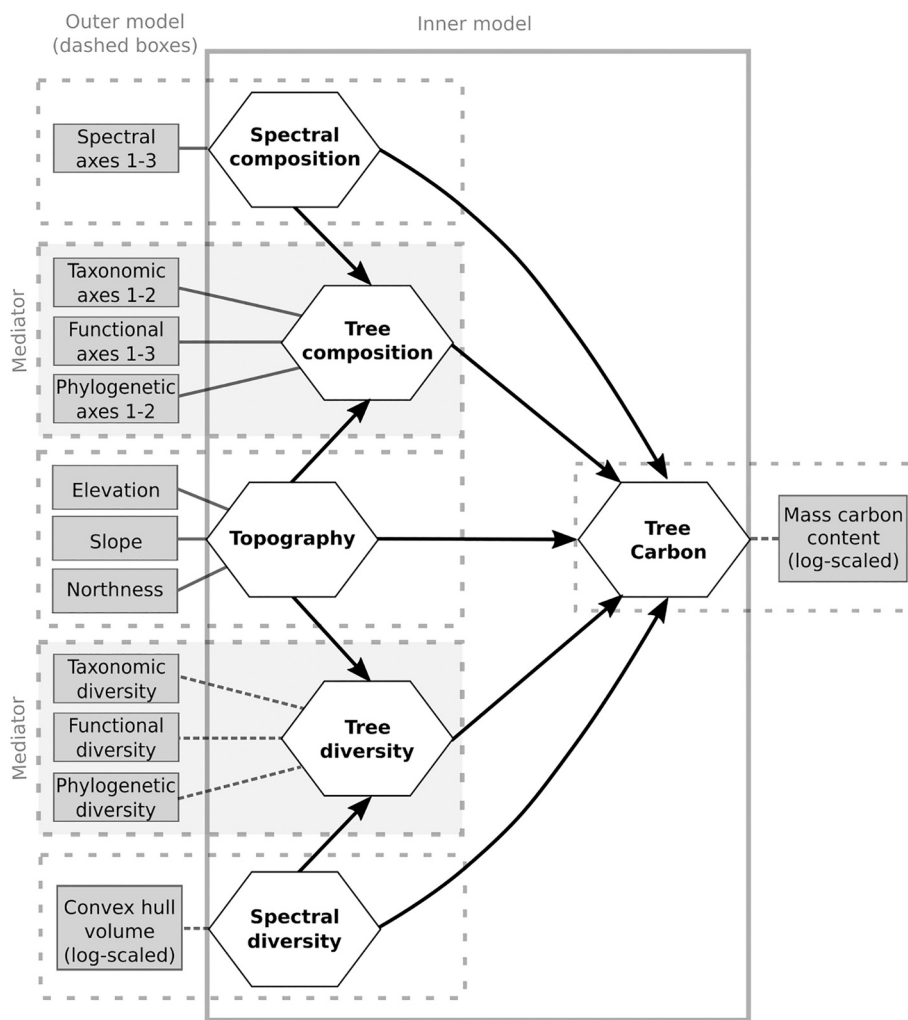


Fig. 2. A priori path model for explaining tree carbon content considering all direct and indirect paths with the independent constructs topography, hyperspectral composition and hyperspectral diversity, as well as the potential mediators tree composition, and tree diversity (gray boxes). All ordination axes were considered as individual indicator variables. Elevation was quantified in m a.s.l., slope in degrees, mass carbon content in $t\ ha^{-1}$. Inner and outer models are shown by solid and dashed boxes, respectively. Solid lines in the outer model illustrate formative concepts and dashed lines indicate reflective concepts. Single variables in the outer model are always considered reflective. See Hair et al. (2021a) for modeling methods and terminology.

taxonomic, functional and phylogenetic composition largely driven by differences in coniferous species and angiosperms. Functional axis 1 indicated inter-correlated leaf traits, such as leaf pigments and structural and chemical traits (e.g., SLA, LMA, C and N content; Fig. 4 c); however, such information cannot be obtained from the phylogenetic axis 1. In addition to taxonomic turnover, functional axis 2 ($w = -0.23$, $p < 0.001$), and functional axis 3 ($w = 0.12$, $p < 0.1$; Fig. 3 a) showed a weaker but still significant contribution to tree composition, indicating variations in carbon fractions as well as the water-related traits leaf dry matter content (LDMC) and leaf water content (LWC).

For topography, elevation and slope were both significant but with a higher relative contribution of elevation ($w = 1.05$, $p < 0.001$). All tree species diversity metrics fulfilled the criteria for reflective constructs and were highly significant ($p < 0.001$) with the highest contribution from phylogenetic diversity ($w = 0.42$, $p < 0.001$, Fig. 3 b).

3.2. Direct and indirect effects in modeling forest C content

For both topography and hyperspectral composition, we found strong indirect paths to C content via tree composition after bootstrapping. For spectral composition as well as for topography we identified a full mediation as the direct paths to C content were not significant. Spectral diversity, in turn, did not influence C content via a direct or indirect pathway. Although there was a significant relationship to tree diversity ($\beta = 0.67$, $p < 0.001$), the path from tree species diversity to C content was weak and not significant (Fig. 3 b), indicating no mediation of spectral diversity and C content by tree diversity. In

addition, tree diversity did not mediate the relationship between topography and C content. We further extracted the scores of constructs from the full path model (Fig. 3), with Fig. 5 showing their pairwise correlations and links to conifer content (in %).

3.3. Explanatory and predictive power

Carbon content was explained to a moderate degree (58%), and most explanatory power was derived from spectral composition and topography, with strong indirect paths through tree composition. Spectral composition and topography together explained 82% of the variation in tree composition between plots, whereas only 45% of the variation in tree diversity was explained by spectral diversity.

After the removal of insignificant paths, we found that the path model had a lower out-of-sample predictive error for C content (RMSE = 0.272) compared to a linear model using all indicator variables (i.e., spectral axes 1, 3, 5, elevation and slope, taxonomic axis 1 and functional axes 2, 3) as predictors (RMSE = 0.307). The better performance of the path model indicated a high predictive power.

3.4. Additional path models

Given some degree of correlation between the antecedent constructs (spectral composition, topography, and spectral diversity) in the path model in Fig. 3, we also ran separate path models using either the composition or diversity variables and removing topography as a predictor. This was done to quantify the variation in C content that could be

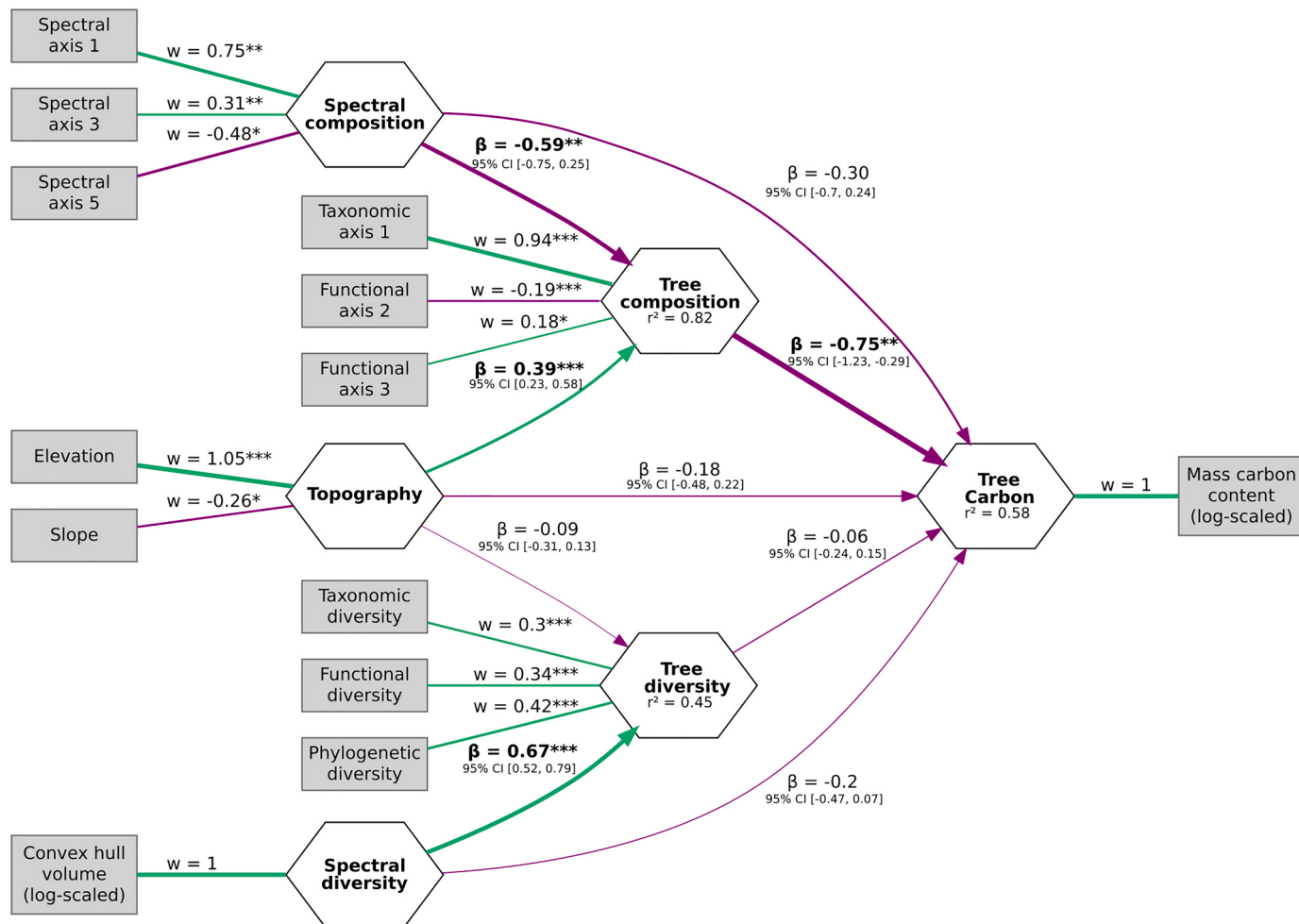


Fig. 3. Final validated and bootstrapped inner and outer path model for C content, with the direct paths from spectral composition, topography, and spectral diversity to C content, and the indirect paths via tree species composition and tree species diversity. Lines and arrows in magenta indicate negative effects, green arrows positive effects. Line width is scaled proportional to effect size (β) or the indicator weight (w). Confidence intervals and significance of paths were determined by bootstrapping (10,000 iterations). Effect sizes of significant paths are shown in bold. Indicator variables were removed due to high multicollinearity or low relevance within constructs (see supplementary data; Hair et al., 2021a). Single indicator variables as well as the variables in tree diversity were reflectively measured, all other variables formatively (see Methods). (For interpretation of the references to colour in this figure legend, the reader is referred to the web version of this article.)

explained by either spectral composition and species composition of trees or spectral diversity and species diversity of trees (Fig. 6). Consistent with the full model, we found that tree composition mediated the spectral composition - C content relationship, but with higher effect sizes, significance levels, and still explaining up to 51% in C content (Fig. 6 a). Tree diversity, in turn, did not mediate the spectral diversity - C content relationship. However, in contrast to the full model, spectral diversity was directly related to C content ($\beta = -0.44$, $p < 0.01$), explaining 20% in C content (Fig. 6 b).

4. Discussion

We analyzed the direct and indirect relationships among hyperspectral data, canopy properties (composition and diversity) and C content. Our findings revealed that C content was mainly influenced by the coupled changes of taxonomic, functional, and phylogenetic tree composition, which were successfully captured by spectral composition (the average reflectance per plot; Fig. 4 a). Meanwhile, the influence of spectral diversity on C content was low and not mediated by tree diversity in these two studied forests in Quebec, Canada. All results were strongly influenced by a gradient from deciduous to coniferous trees with increasing elevation.

4.1. Spectral composition, tree composition and its links to C content

The transition from deciduous to coniferous tree species played a major role, shaping the taxonomic, functional and phylogenetic composition across plots. Tree composition showed strong links to the leaf-economics spectrum, LES (Reich et al., 1997; Wright et al., 2004), indicating fast to slow plant strategies, as well to phylogenetic composition, specifically a gradient between forests dominated by gymnosperms or angiosperms. In general, deciduous tree reflectance is higher than the reflectance of conifer species in the NIR, and SWIR regions (Appendix A Fig. A2; Ollinger, 2011; Ollinger and Smith, 2005; Williams, 1991). Ollinger (2011) argued that this difference in canopy reflectance is due to the combined effects of canopy structure and leaf traits.

Canopy reflectance can be affected by the pyramidal structure of conifer crowns vs. more rounded crowns in broadleaved trees (Rautiainen et al., 2004). As suggested by Serbin and Townsend (2020), we used continuum removal to diminish illumination differences across different flight lines as well as canopy structural effects to derive normalized spectra that differ less between conifers and broadleaf species (Appendix A Fig. A2). However, some visual differences in reflectance can persist, as we found in our study (see supplementary data). Also, effects from internal scattering due to canopy structural effects can

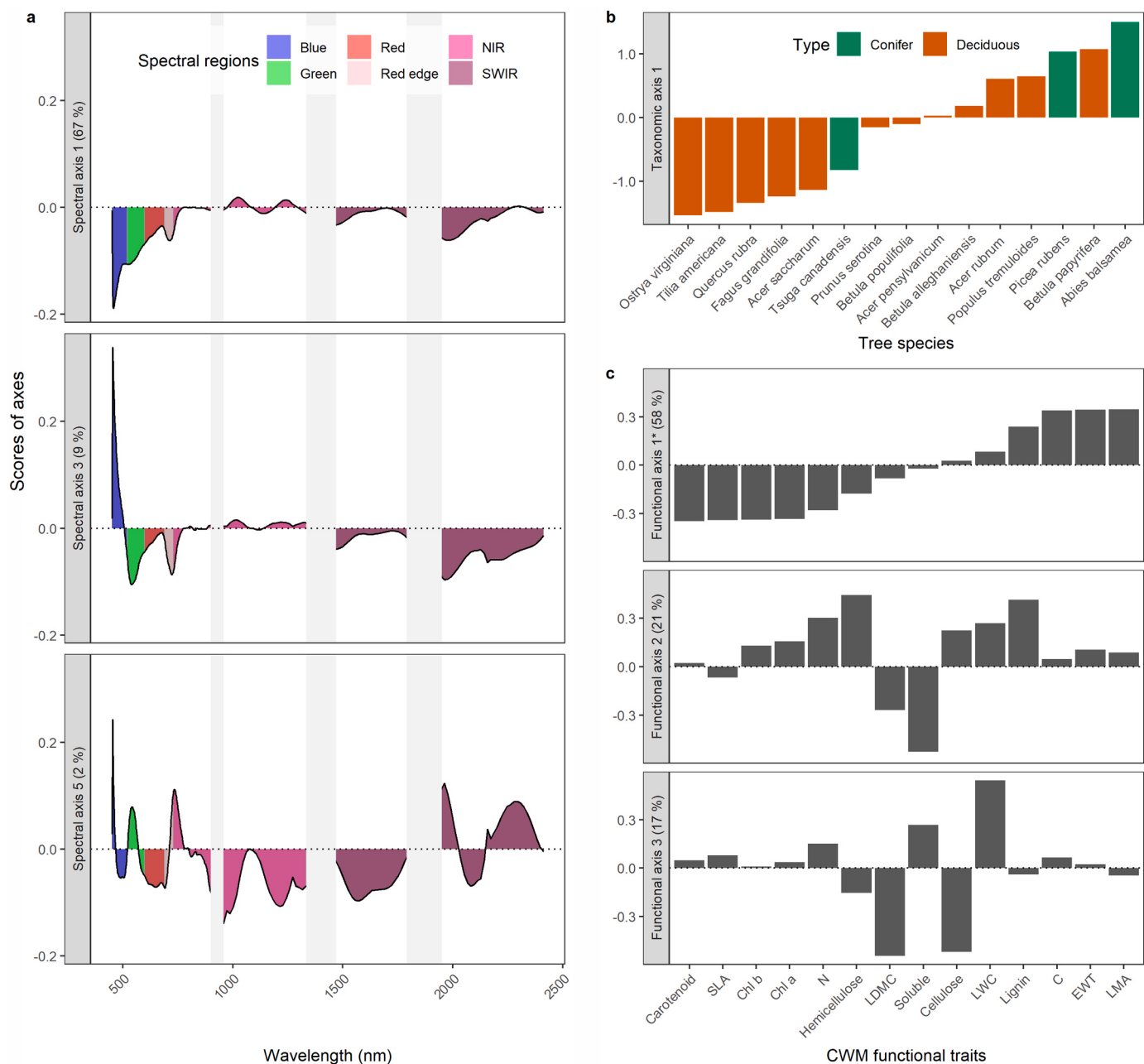


Fig. 4. Significant indicators of tree composition and their ordination scores for (a) spectral wavelength bands (continuum-removed reflectance) within the three selected spectral axes, (b) tree species within the first taxonomic axis (shown are the 15 most abundant tree species), and (c) CWM traits within the first three functional axes. Spectral regions are divided into blue (< 520 nm), green (520–600 nm), red (600–690 nm), red edge (690–730 nm), near infrared (NIR; 730–1400 nm) and shortwave infrared (SWIR; >1400 nm). Noisy bands and water absorption bands were masked out (gray areas). C = leaf carbon, Chl = chlorophyll, ETW = Equivalent water thickness, LDMC = leaf dry matter content, LMA = leaf mass per area, LWC = leaf water content, N = leaf nitrogen, SLA = specific leaf area. Units of functional traits are given in Appendix A Table A1. (For interpretation of the references to colour in this figure legend, the reader is referred to the web version of this article.)

* Functional axis 1 has been removed from the path model due to high correlation to taxonomic axis 1 (Appendix A Fig. A1).

result in an increased depth of absorption features (Ollinger, 2011).

Regardless of canopy structural effects, deciduous and coniferous trees differ in their functional traits, which can successfully be predicted by hyperspectral data. Singh et al. (2015) predicted multiple functional traits related to the LES along a deciduous-coniferous gradient, with highest performance for leaf mass per area ($r^2 = 0.88$) and % N content ($r^2 = 0.84$). In line with previous studies, we found that mostly the visible bands (spectral axis 1) and multiple absorption features (spectral axis 5) capture differences in tree composition. This appears to be due to associations with leaf pigments (Asner et al., 2015), and other chemical

traits, such as cellulose, EWT, and LDMC (Ollinger, 2011), with the potential to discriminate deciduous and coniferous tree species (Hovi et al., 2017). Overall, the path models (Figs. 3, 6) explained >80% in tree composition, indicating a strong link between hyperspectral data and tree composition, as also found in previous studies; e.g., along a vegetation gradient in a woody savannah ecosystem ($r^2 = 0.7$; Leitão et al., 2019), a walnut-fruit forests in Kyrgyzstan, Central Asia ($r^2 = 0.59$ –0.63, Feilhauer and Schmidlein, 2009), or a forest ecosystem in North Carolina, USA ($r^2 = 0.71$, together with elevation; Hakkenberg et al., 2018).

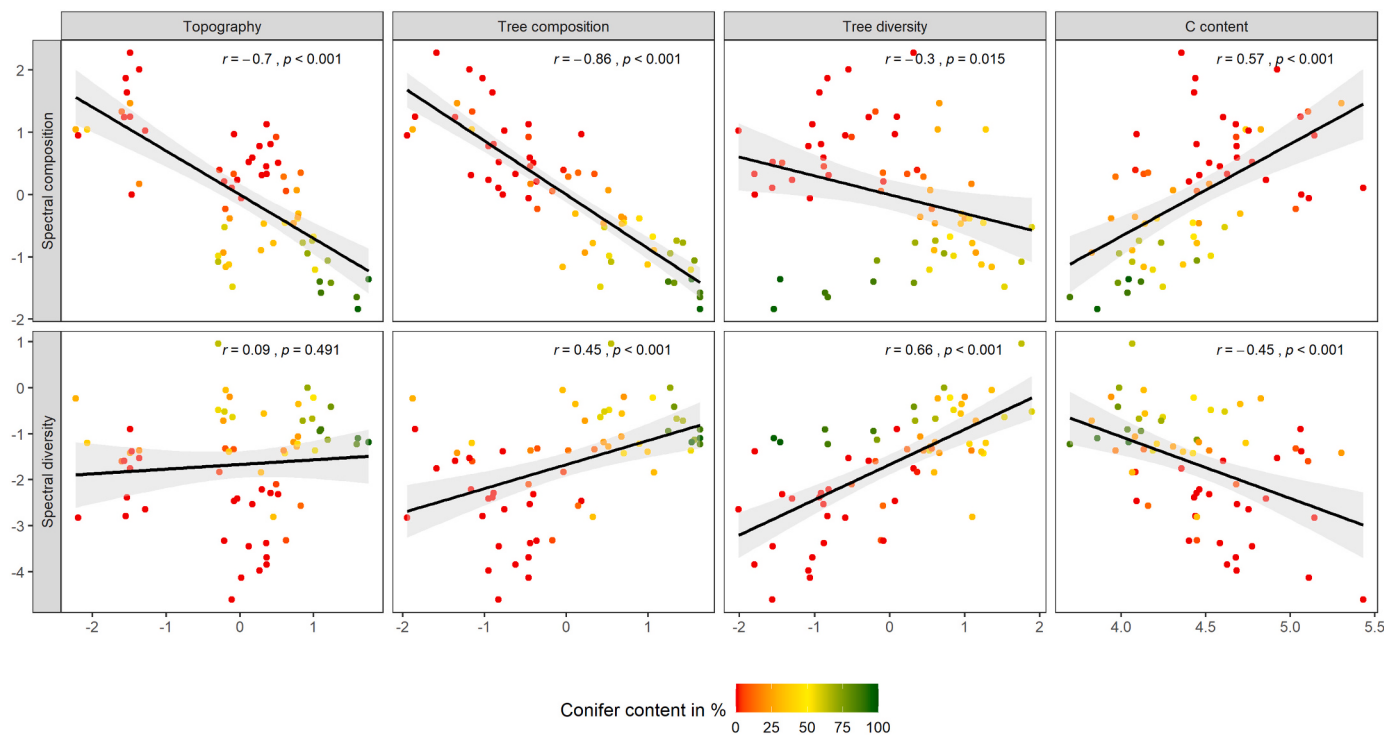


Fig. 5. Pairwise correlations (Pearson's product moment coefficient) between constructs. Scores are from the final path model constructs tree composition, tree diversity, spectral composition and topography (shown in Fig. 3). The single-item constructs spectral diversity and C content are log-scaled. The percentage conifer content per plot is shown by colour.

Our findings also suggest that composition is a major driver of ecosystem functions, indicating higher C content in forest stands with more deciduous species at lower elevations, which generally have higher values of chlorophyll *a* and *b*. This is supported by prior studies showing how trait composition in forests relates to ecosystem functions. For instance, Ollinger and Smith (2005) showed that estimates of N concentrations could successfully predict forest composition (fraction of deciduous and evergreen species, $r^2 = 0.72$) as well as stand productivity ($r^2 = 0.70\text{--}0.74$) in a temperate forest in New Hampshire, USA. These results suggest an indirect relationship of hyperspectral reflectance and ecosystem functions via tree composition.

4.2. Spectral diversity, tree diversity and its links to C content

The ability to predict tree diversity from spectral diversity was only moderate, but indicated a positive and significant trend with higher tree diversity at plots with higher spectral diversity (using the convex hull volume, CHV; Appendix Fig. A3). CHV, however, has not always performed well in previous studies and has been criticized because it is based on the range of values (Dahlin, 2016), which is sensitive to extreme values and outliers. To assess the robustness of our conclusions to the choice of spectral diversity metric, we also tested the squared distance to the centroid, a spectral metric described in Laliberté et al. (2020), as well as the convex hull area, introduced in Gholizadeh et al. (2018). For both models, the predictability of tree species diversity decreased compared to the model using the CHV. The convex hull area explained more variation in C content via a direct pathway but at the same time explained <20% of variance in tree diversity (Appendix A Fig. A4). We assume that the averaging of spectral points within tree crowns mostly eliminated extreme values and large outliers, which might have made the CHV a more robust measure of spectral diversity.

While the majority of spectral diversity studies has been done in grasslands, evidence for a strong positive spectral diversity – tree diversity relationship is mixed. In lowland tropical rainforests, spectral diversity has been shown to effectively estimate species richness of

emergent trees with an r^2 of 0.56 (Jucker et al., 2018). Féret and Asner (2014) showed strong links between spectral diversity and tropical tree canopy diversity ($r = 0.86, p < 0.00$). Carlson et al. (2007) showed that the reflectance ranges (as a measure of spectral variation) of airborne hyperspectral data were significantly related to tree species richness in a lowland rainforest (85%). However, given the wide range of spectral diversity metrics but limited number of comparative studies in temperate or boreal forest ecosystems, a more systematic analysis is needed to explore the conditions under which spectral diversity metrics might contribute to modeling and monitoring tree diversity (see also Fassnacht et al., 2022).

Our findings also suggest that tree diversity has no detectable effect on C content. This is in line with studies indicating that C content or AGB are not related to species richness (Adler et al., 2011) or trait diversity (Finegan et al., 2015), although it runs counter to many observational studies reporting positive relationships between diversity and above-ground C storage (Liu et al., 2018) or other ecosystem functions (Albrecht et al., 2021; Paquette and Messier, 2011). The direct link from spectral diversity to C content in the diversity-only model (Fig. 6 b) suggests that there are mediators that we did not measure. This interpretation is supported by multiple studies suggesting that airborne spectral reflectance and its diversity captures not only plant diversity, but also structural information from the canopy (Ollinger, 2011; Schweiger et al., 2018). There are further potential mediators that we did not consider in this study, such as soil conditions, since our objective was to analyze tree compositional and diversity effects on C content using hyperspectral data.

4.3. Transferability and implications at different spatial and spectral scales

While our aim was to enhance our knowledge about the indirect relationships between optical remote sensing and C content, the same methods could be used with a combination of hyperspectral data and crown delineation from lidar data (Zhao et al., 2018). However, our

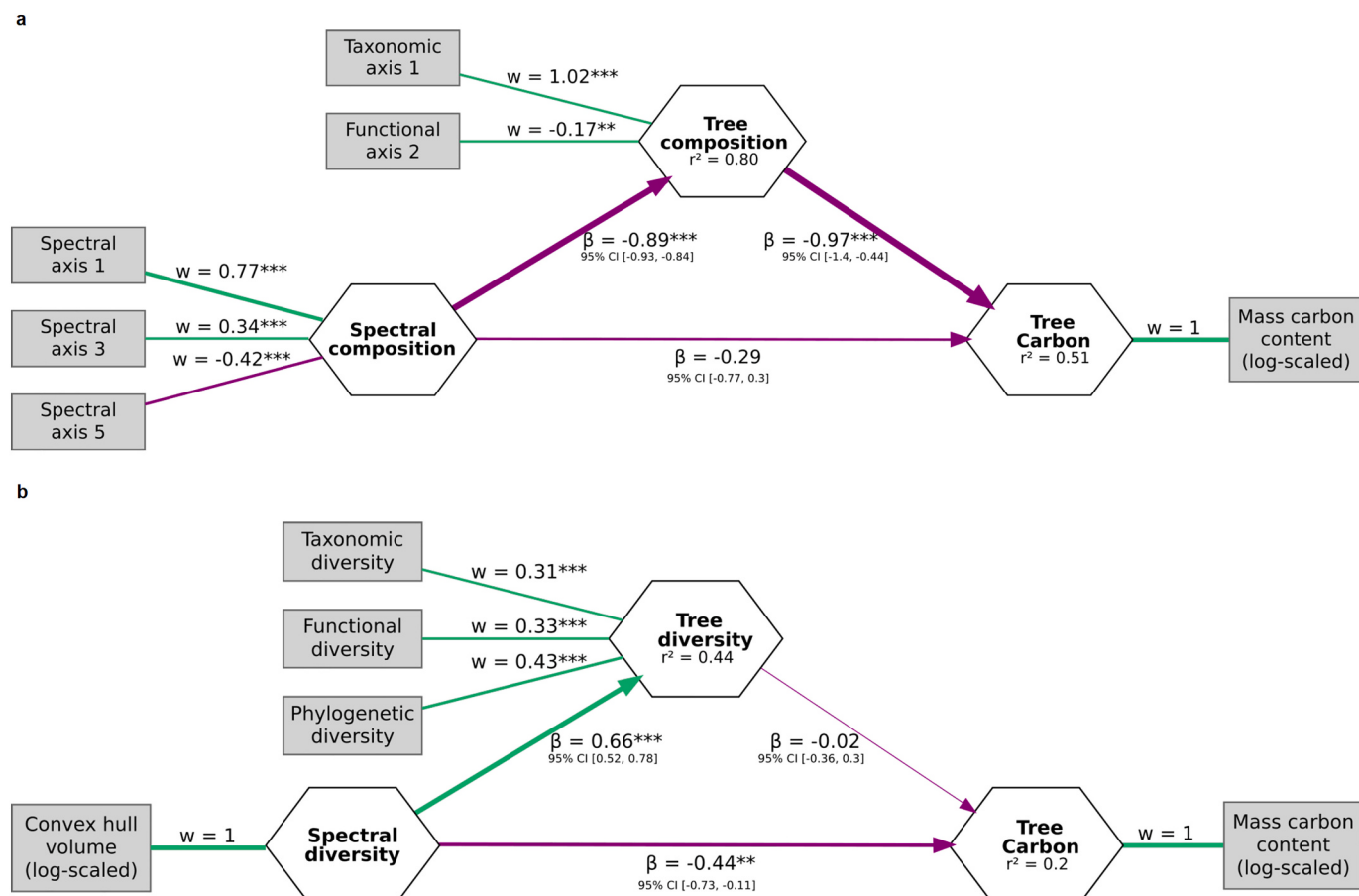


Fig. 6. Separate path models for C content based on (a) spectral composition and tree species composition, and (b) spectral diversity and tree species diversity. Functional axis 3 in (a) has been removed because of an insignificant weight. See Fig. 3 for further information.

results also suggest that the average reflectance per plot is a better predictor of C content than spectral diversity and we were able to identify spectral regions of interest for C content estimations in the VIS, NIR, and SWIR regions. These wavelength regions are covered by spaceborne sensors that have coarser spectral and spatial resolutions, such as on-board Sentinel-2 launched by the European Space Agency (<https://sentinel.esa.int/web/sentinel/missions/sentinel-2>; Phiri et al., 2020) or the joint NASA/USGS Landsat program (Wu et al., 2019). Considering sensors from the Landsat or Sentinel mission, the spatial resolution of pixels range between 10 and 60 m depending on the wavelengths, and therefore, these sensors capture average stand-level spectra that are primarily influenced by dominant canopy tree species composition. Multiple remote sensing studies showed that such data at moderate spectral and spatial resolution is able to estimate ecosystem functions such as tropical forest AGB or productivity along an environmental gradient (e.g., Wallis et al., 2019). Comparing multiple spaceborne sensors, Naik et al. (2021) found a significant increase in AGB model performance when using data from the red edge and SWIR channels. Using Sentinel-2 data, they were able to explain up to 53% (cross-validated r^2) in forest AGB in Trento, Italy. This is comparable to the explained variance of C content (58%) found in our study using

spectral composition and topography as predictors, and it further supports our assumption that optical remote sensing data at moderate spatial resolution capture the average spectral signal of a tree community, which we have shown is associated with changes in tree composition, and in turn with ecosystem functions.

5. Conclusion

Overall, we found that spectral composition in forest plots (the average reflectance) is a better predictor of C content than spectral diversity. We analyzed the underlying mechanisms and showed that the vast majority of these relationships were mediated by the coupled taxonomic, functional, and phylogenetic turnover in tree composition, mostly driven by a change from deciduous to coniferous species. In contrast, tree diversity did not mediate the spectral diversity – C content relationship, and the direct effect of spectral diversity on C content was only moderate. We conclude that direct estimations of C content by spectral data can, therefore, be explained by the tree composition at the canopy scale and suggest that this indirect relationship is also present for spectral data at broader spectral and spatial resolutions.

CRediT authorship contribution statement

Christine I.B. Wallis: Conceptualization, Formal analysis, Visualization, Software, Writing – original draft, Methodology, Investigation, Resources, Data curation, Writing – review & editing. **Anna L. Crofts:** Conceptualization, Methodology, Investigation, Resources, Data curation, Writing – review & editing. **Deep Inamdar:** Methodology, Investigation, Resources, Data curation, Writing – review & editing. **J. Pablo Arroyo-Mora:** Methodology, Investigation, Resources, Data curation, Writing – review & editing. **Margaret Kalacska:** Methodology, Investigation, Resources, Data curation, Writing – review & editing, Funding acquisition. **Étienne Laliberté:** Conceptualization, Methodology, Investigation, Resources, Data curation, Writing – review & editing, Supervision, Project administration, Funding acquisition. **Mark Vellend:** Conceptualization, Methodology, Investigation, Resources, Data curation, Writing – review & editing, Supervision, Funding acquisition.

Declaration of Competing Interest

The authors declare that they have no known competing financial interests or personal relationships that could have appeared to influence the work reported in this paper.

Appendix A

Table A1

Summary statistics of C content and functional leaf traits (rounded to two digits). AGB = Above-ground biomass.

	Variable	Abbreviation	unit	mean	min	max
Tree C content	AGB carbon content	C content	t ha ⁻¹	96.39	39.16	228.62
CWM leaf traits	Carbon content (leaf)	C	%	48.48	46.85	50.94
	Carotenoids	Carotenoids	mg g ⁻¹	0.512	0.31	0.69
	Cellulose	Cellulose	%	10.69	9.47	13.97
	Chlorophyll a	Chl a	mg g ⁻¹	2.49	1.47	3.26
	Chlorophyll b	Chl b	mg g ⁻¹	0.84	0.50	1.23
	Equivalent water thickness	EWT	cm	0.01	0.01	0.02
	Hemicellulose	Hemicellulose	%	11.18	8.42	16.72
	Leaf dry matter content	LDMC	mg g ⁻¹	410.10	374.40	453.90
	Leaf mass per area	LMA	g m ⁻²	103.97	56.42	196.73
	Leaf water content	LWC	mg g ⁻¹	589.90	546.10	625.60
	Lignin	Lignin	%	8.73	6.40	10.79
	Nitrogen content	N	%	1.83	1.34	2.25
	Soluble content	Soluble	%	69.06	60.91	73.87
	Specific leaf area	SLA	m ² kg ⁻¹	13.47	5.43	18.95

Table A2

Airborne hyperspectral data collection.

Mont Mégantic					Mont-Saint-Bruno				
	Recording time of day	Height (above sea level)	Speed	Spatial resolution along track	Recording time of day	Height (above sea level)	Speed	Spatial resolution along track	Spatial resolution across track
CASI	2019/07/18 14:35–15:28 (GMT)	3123 m	51.4 m/s	2.47 m	1.16 m	2018/09/08 14:59 (GMT)	1680 m	39.1 m/s	0.79 m (1.58 m after summation)
SASI	2019/07/18 14:35–15:28 (GMT)	3123 m	51.4 m/s	2.71 m	2.71 m	2018/09/08 14:59 (GMT)	1680 m	39.1 m/s	1.83

Data availability

Data will be made available on request.

Acknowledgements

This study was conducted in the framework of the CABO project, funded by the Natural Sciences and Engineering Research Council of Canada (509190-2017). We would like to thank the many field and laboratory assistants for their help in conducting the forest inventory surveys and leaf sampling, and in quantifying foliar traits. In particular, we would like to recognize Sabrina Demers-Thibeault who led the leaf sampling and foliar trait quantification effort and Sabine St-Jean for her contribution to the forest inventories. We additionally like to thank Raymond Soffer from the National Research Council Canada (NRC) for his help with the preprocessing of the hyperspectral data. We thank the staff in Parc national du Mont Mégantic and in Parc national du Mont-Saint-Bruno for facilitating access to the field sites and their ongoing support. We are grateful to three anonymous reviewers and an associate editor for critical suggestions that significantly improved the manuscript.

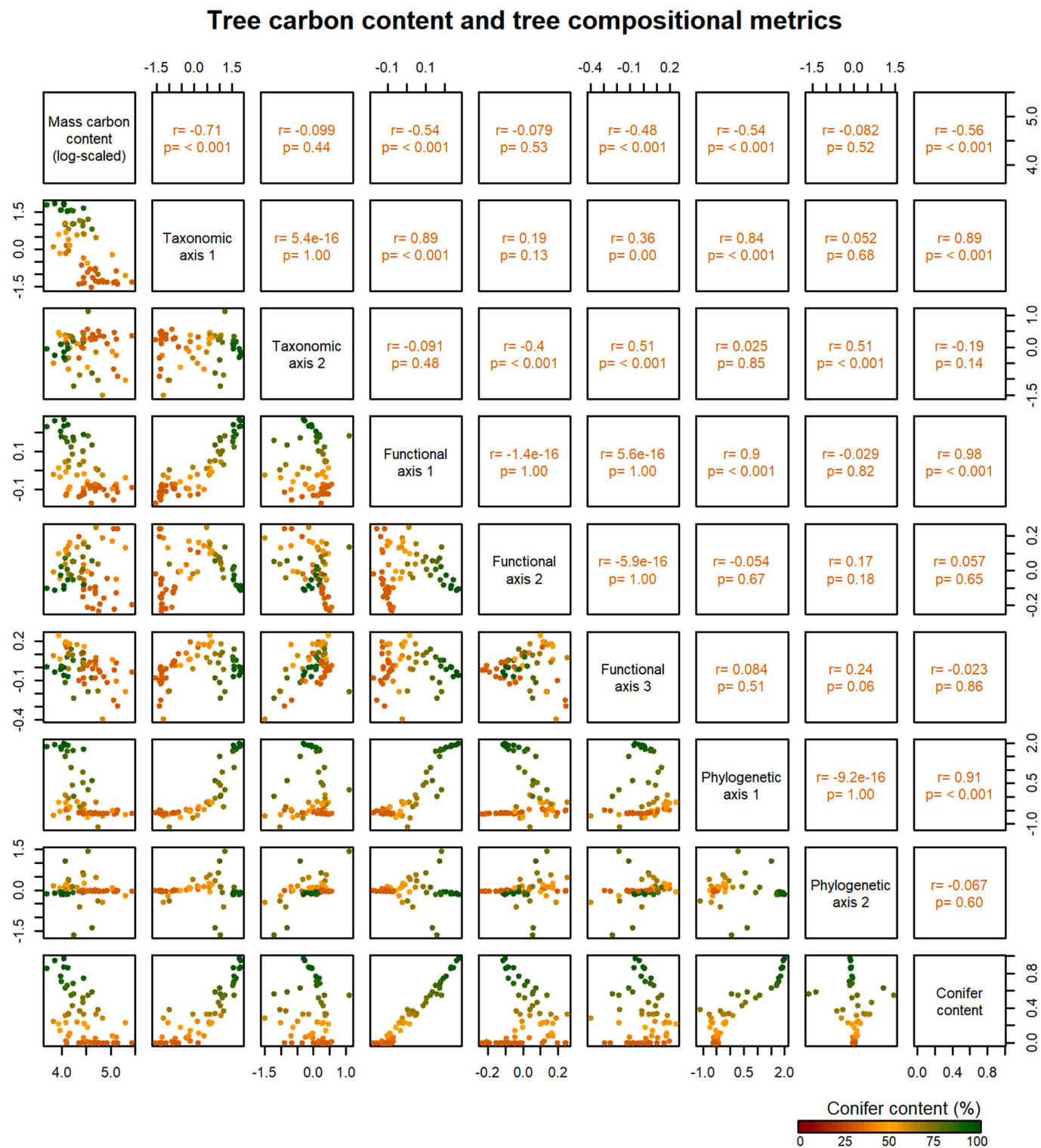


Fig. A1. Scatterplot matrix of C content and tree compositional variables from the taxonomic, functional and phylogenetic domains by means of ordinations as well as the plot-wise conifer content. Correlations are based on the Pearson correlation moment (r) and corresponding p -values.

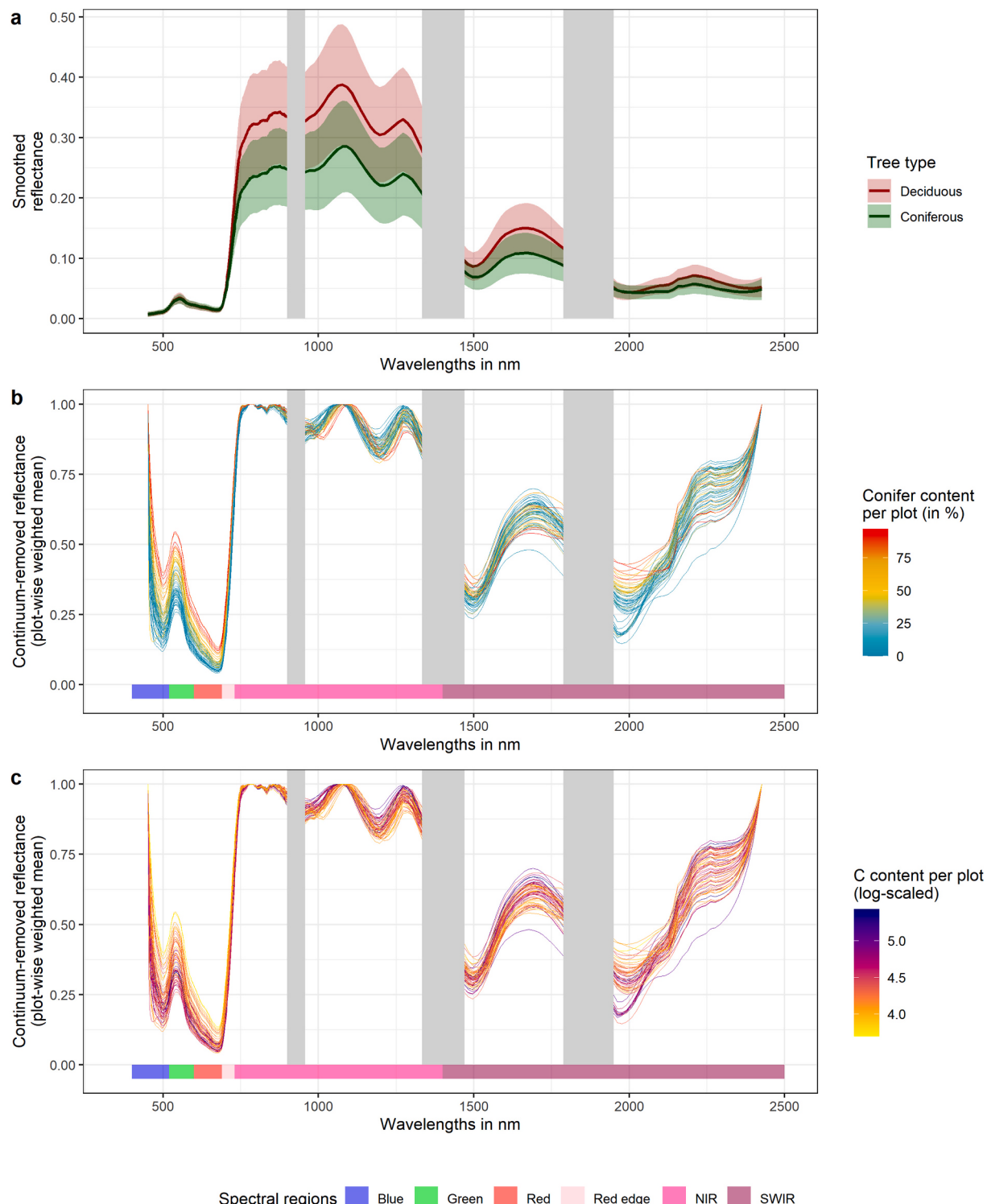


Fig. A2. a) The smoothed reflectance of tree individuals grouped by deciduous and coniferous species. Below, the averaged continuum-removed spectrum for each plot. Lines are colored by b) the percentage conifer content per plot and c) the log-scaled C content per plot. The mean of spectral points per plot has been weighted by the corresponding crown size. Gray areas indicate spectral regions that have been masked out due to noisy bands or water absorption.

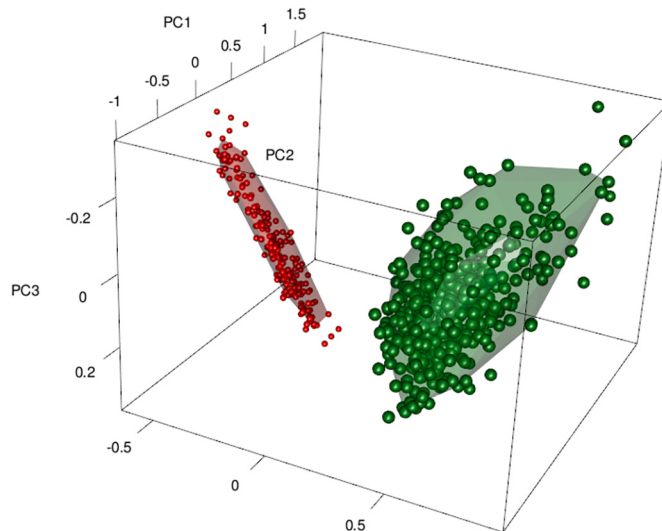


Fig. A3. Convex hull volume of the first three spectral PCs for two exemplary plots with low spectral diversity in red and high spectral diversity in green. (For interpretation of the references to colour in this figure legend, the reader is referred to the web version of this article.)

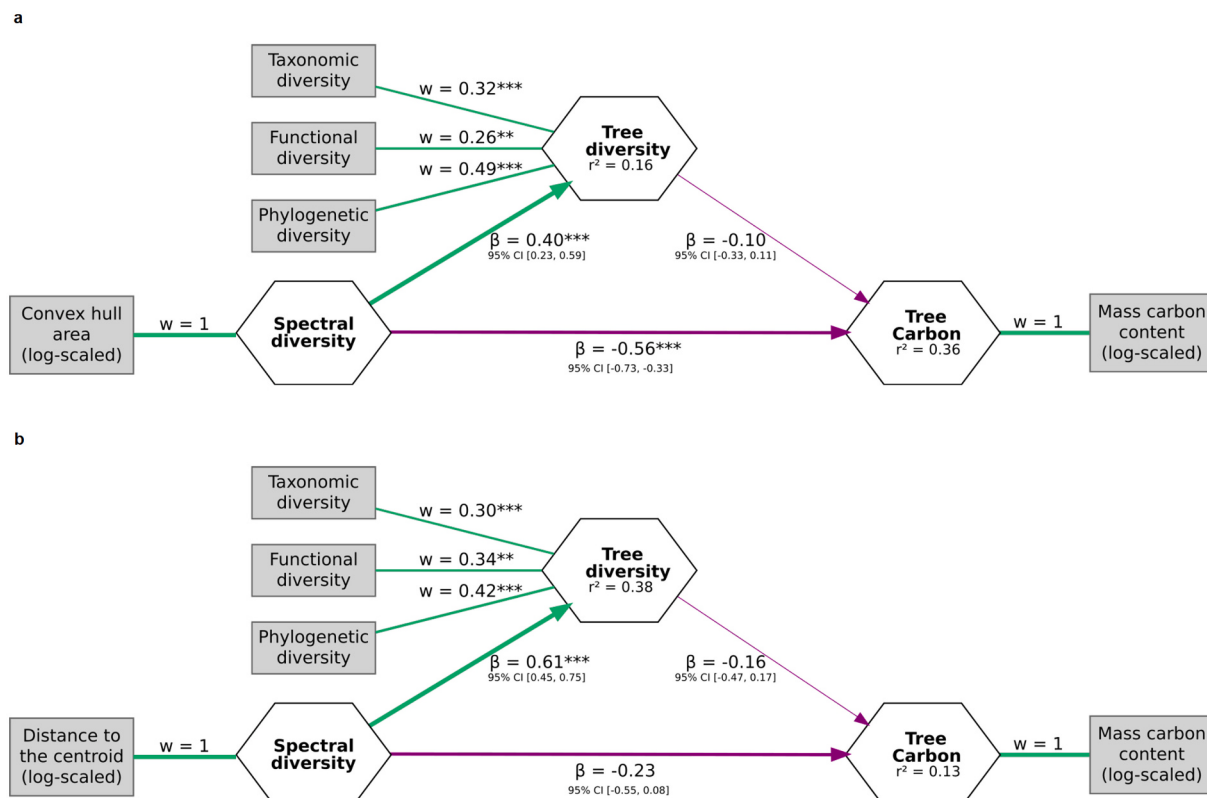


Fig. A4. Path models using the (a) convex hull area and (b) squared distance to the centroid of the spectral axes instead of the convex hull volume as a spectral diversity metric.

Appendix A. Supplementary data

Supplementary data to this article can be found online at <https://doi.org/10.1016/j.rse.2022.113333>.

References

- Adler, P., Seabloom, E., Borer, E., Hillebrand, H., Hautier, Y., Hector, A., Harpole, W., O'Halloran, L., Grace, J., Anderson, T., Bakker, J., Biederman, L., Brown, C., Buckley, Y., White, L., Chu, C., Cleland, E., Collins, S., Cottingham, K., Yang, L., 2011. Productivity is a poor predictor of plant species richness. *Science* 333, 1750–1753. <https://doi.org/10.1126/science.1204498>.

- Albrecht, J., Peters, M.K., Becker, J.N., Behler, C., Classen, A., Ensslin, A., Ferger, S.W., Gebert, F., Gerschlauer, F., Helbig-Bonitz, M., Kindketa, W.J., Kühnel, A., Mayr, A.V., Njovu, H.K., Pabst, H., Pommer, U., Röder, J., Rutten, G., Schellenberger, Costa, D., Sierra-Cornejo, N., Vogeler, A., Vollstädt, M.G.R., Dulle, H.I., Eardley, C.D., Howell, K.M., Keller, A., Peters, R.S., Kakengi, V., Hemp, C., Zhang, J., Manning, P., Mueller, T., Bogner, C., Böhning-Gaese, K., Brandl, R., Hertel, D., Huwe, B., Kiese, R., Kleyer, M., Leuschner, C., Kuzyakov, Y., Nauss, T., Tschapka, M., Fischer, M., Hemp, A., Steffan-Dewenter, I., Schleuning, M., 2021. Species richness is

- more important for ecosystem functioning than species turnover along an elevational gradient. *Nat. Ecol. Evol.* 5, 1582–1593. <https://doi.org/10.1038/s41559-021-01550-9>.
- Almeida, D.R.A.de, Broadbent, E.N., Ferreira, M.P., Meli, P., Zambrano, A.M.A., Gorgens, E.B., Resende, A.F., de Almeida, C.T., do Amaral, C.H., Corte, A.P.D., Silva, C.A., Romanelli, J.P., Prata, G.A., de Almeida Papa, D., Stark, S.C., Valbuena, R., Nelson, B.W., Guillemot, J., Féret, J.-B., Chazdon, R., Brancalion, P.H.S., 2021. Monitoring restored tropical forest diversity and structure through UAV-borne hyperspectral and lidar fusion. *Remote Sens. Environ.* 264, 112582. <https://doi.org/10.1016/j.rse.2021.112582>.
- Asner, G., Knapp, D., Anderson, C., Martin, R., Vaughn, N., 2016. Large-scale climatic and geophysical controls on the leaf economics spectrum. *Proc. Natl. Acad. Sci.* 113, 201604863. <https://doi.org/10.1073/pnas.1604863113>.
- Asner, G.P., Martin, R.E., Anderson, C.B., Knapp, D.E., 2015. Quantifying forest canopy traits: imaging spectroscopy versus field survey. *Remote Sens. Environ.* 158, 15–27. <https://doi.org/10.1016/j.rse.2014.11.011>.
- Ayotte, J., Laliberté, E., 2019. Measuring leaf carbon fractions with the ANKOM2000 Fiber Analyzer [WWW Document]. protocols.io. URL (accessed 2.2.22). <https://www.protocols.io/view/measuring-leaf-carbon-fractions-with-the-anko-m2000-yinfude>.
- Benitez, J., Henseler, J., Castillo, A., Schuberth, F., 2020. How to perform and report an impactful analysis using partial least squares: guidelines for confirmatory and explanatory IS research. *Inf. Manag.* 57, 103168 <https://doi.org/10.1016/j.im.2019.05.003>.
- Cadotte, M.W., 2017. Functional traits explain ecosystem function through opposing mechanisms. *Ecol. Lett.* 20, 989–996. <https://doi.org/10.1111/ele.12796>.
- Cadotte, M.W., Carscadden, K., Mirochnick, N., 2011. Beyond species: functional diversity and the maintenance of ecological processes and services. *J. Appl. Ecol.* 48, 1079–1087.
- Cadotte, M.W., Cavender-Bares, J., Tilman, D., Oakley, T.H., 2009. Using phylogenetic, functional and trait diversity to understand patterns of plant community productivity. *PLOS ONE* 4, e5695. <https://doi.org/10.1371/journal.pone.0005695>.
- Carlson, K.M., Asner, G.P., Hughes, R.F., Ostertag, R., Martin, R.E., 2007. Hyperspectral remote sensing of canopy biodiversity in hawaiian lowland rainforests. *Ecosystems* 10, 536–549. <https://doi.org/10.1007/s10021-007-9041-z>.
- Carteron, A., Paraguive, V., Blanchard, F., Guilbeault-Mayers, X., Turner, B.L., Vellend, M., Laliberté, E., 2020. Soil abiotic and biotic properties constrain the establishment of a dominant temperate tree into boreal forests. *J. Ecol.* 108, 931–944. <https://doi.org/10.1111/1365-2745.13326>.
- Castillo, J.A.A., Apan, A.A., Maraseni, T.N., Salmo, S.G., 2017. Estimation and mapping of above-ground biomass of mangrove forests and their replacement land uses in the Philippines using sentinel imagery. *ISPRS J. Photogramm. Remote Sens.* 134, 70–85. <https://doi.org/10.1016/j.isprsjprs.2017.10.016>.
- Cavender-Bares, J., Meireles, J.E., Couture, J.J., Kaproth, M.A., Kingdon, C.C., Singh, A., Serbin, S.P., Center, A., Zuniga, E., Pilz, G., Townsend, P.A., 2016. Associations of leaf spectra with genetic and phylogenetic variation in oaks: prospects for remote detection of biodiversity. *Remote Sens.* 8, 221. <https://doi.org/10.3390/rs8030221>.
- Cepeda-Carrion, G., Nitzl, C., Roldán, J., 2018. Mediation analyses in partial least squares structural equation modeling: guidelines and empirical examples. In: Partial Least Squares Path Modeling: Basic Concepts, Methodological Issues and Applications. https://doi.org/10.1007/978-3-319-64069-3_8.
- Core, R., Team, R., 2020. A language and environment for statistical computing, R Foundation for Statistical Computing; 201.
- Cornwell, W.K., Schwilk, D.W., Ackerly, D.D., 2006. A trait-based test for habitat filtering: convex hull volume. *Ecology* 87, 1465–1471. [https://doi.org/10.1890/0012-9658\(2006\)87\[1465:ATTFHF\]2.0.CO;2](https://doi.org/10.1890/0012-9658(2006)87[1465:ATTFHF]2.0.CO;2).
- Crockett, E.T.H., Vennin, S., Botzas-Coloni, J., Larocque, G., Bennett, E.M., 2021. Bright spots of carbon storage in temperate forests. *J. Appl. Ecol.* 58, 3012–3022. <https://doi.org/10.1111/1365-2664.14042>.
- Crofts, A.L., St-Jean, S., 2022. Tree Mapping for Leaf Collection Guidelines (Mont Mégaantic only) [WWW Document]. protocols.io. URL (accessed 9.13.22). <https://www.protocols.io/view/tree-mapping-for-leaf-collection-guidelines-mont-m-ccqcsvsw>.
- Crofts, A.L., St-Jean, S., Vellend, M., 2022. Canadian Airborne Biodiversity Observatory's Forest Inventory Field Survey Protocol v2 (preprint. <https://doi.org/10.17504/protocols.io.q26g7rn23vww/v2>.
- Curran, P.J., 1989. Remote sensing of foliar chemistry. *Remote Sens. Environ.* 30, 271–278. [https://doi.org/10.1016/0034-4257\(89\)90069-2](https://doi.org/10.1016/0034-4257(89)90069-2).
- Dahlin, K.M., 2016. Spectral diversity area relationships for assessing biodiversity in a wildland-agriculture matrix. *Ecol. Appl.* 26, 2758–2768. <https://doi.org/10.1002/eaap.1390>.
- Environment and Climate Change Canada, 2011. Historical Climate Data - Climate - Environment and Climate Change Canada [WWW Document] accessed 2.11.22. http://climate.weather.gc.ca/index_e.html.
- Fan, Y., Chen, J., Shirkey, G., John, R., Wu, S.R., Park, H., Shao, C., 2016. Applications of structural equation modeling (SEM) in ecological studies: an updated review. *Ecol. Process.* 5, 19. <https://doi.org/10.1186/s13717-016-0063-3>.
- Fasnacht, F.E., Müllerová, J., Conti, L., Malavasi, M., Schmidlein, S., 2022. About the link between biodiversity and spectral variation. *Appl. Veg. Sci.* 25, e12643 <https://doi.org/10.1111/avsc.12643>.
- Feilhauer, H., Schmidlein, S., 2009. Mapping continuous fields of forest alpha and beta diversity. *Appl. Veg. Sci.* 12, 429–439. <https://doi.org/10.1111/j.1654-109X.2009.01037.x>.
- Féret, J.-B., Asner, G.P., 2014. Mapping tropical forest canopy diversity using high-fidelity imaging spectroscopy. *Ecol. Appl.* 24, 1289–1296. <https://doi.org/10.1890/13-1824.1>.
- Finegan, B., Peña-Claros, M., de Oliveira, A., Ascarrunz, N., Bret-Harte, M.S., Carreño-Rocabado, G., Casanoves, F., Díaz, S., Eguiguren Velepucha, P., Fernandez, F., Licona, J.C., Lorenzo, L., Salgado Negret, B., Vaz, M., Poorter, L., 2015. Does functional trait diversity predict above-ground biomass and productivity of tropical forests? Testing three alternative hypotheses. *J. Ecol.* 103, 191–201. <https://doi.org/10.1111/1365-2745.12346>.
- Frye, H.A., Aiello-Lammens, M.E., Euston-Brown, D., Jones, C.S., Kilroy Mollmann, H., Merow, C., Slingsby, J.A., van der Merwe, H., Wilson, A.M., Silander Jr., J.A., 2021. Plant spectral diversity as a surrogate for species, functional and phylogenetic diversity across a hyper-diverse biogeographic region. *Glob. Ecol. Biogeogr.* 30, 1403–1417. <https://doi.org/10.1111/geb.13306>.
- Gholizadeh, H., Gamon, J.A., Zygielbaum, A.I., Wang, R., Schweiger, A.K., Cavender-Bares, J., 2018. Remote sensing of biodiversity: soil correction and data dimension reduction methods improve assessment of α -diversity (species richness) in prairie ecosystems. *Remote Sens. Environ.* 206, 240–253. <https://doi.org/10.1016/j.rse.2017.12.014>.
- Girard, A., Ayotte, J., Laliberté, E., 2021. Measuring chlorophylls and carotenoids in plant tissue [WWW Document]. protocols.io. URL (accessed 2.2.22). <https://www.protocols.io/view/measuring-chlorophylls-and-carotenoids-in-plant-tissue-4g2gtve>.
- Grime, J.P., 1998. Benefits of plant diversity to ecosystems: immediate, filter and founder effects. *J. Ecol.* 86, 902–910. <https://doi.org/10.1046/j.1365-2745.1998.00306.x>.
- Hair, J.F., Hult, G.T.M., Ringle, C.M., Sarstedt, M., Danks, N.P., Ray, S., 2021. Partial Least Squares Structural Equation Modeling (PLS-SEM) Using R: A Workbook. Springer Nature.
- Hair, J.F., Hult, G.T.M., Ringle, C.M., Sarstedt, M., Danks, N.P., Ray, S., 2021. The SEMinR Package. In: Hair Jr., J.F., Hult, G.T.M., Ringle, C.M., Sarstedt, M., Danks, N.P., Ray, S. (Eds.), Partial Least Squares Structural Equation Modeling (PLS-SEM) Using R: A Workbook, Classroom Companion: Business. Springer International Publishing, Cham, pp. 49–74. https://doi.org/10.1007/978-3-030-80519-7_3.
- Hakkenberg, C.R., Peet, R.K., Urban, D.L., Song, C., 2018. Modeling plant composition as community continua in a forest landscape with LiDAR and hyperspectral remote sensing. *Ecol. Appl.* 28, 177–190.
- Hijmans, R.J., Bivand, R., Forner, K., Ooms, J., Pebesma, E., 2021. terra: Spatial Data Analysis.
- Homolová, L., Malenovský, Z., Clevers, J.G.P.W., García-Santos, G., Schaepman, M.E., 2013. Review of optical-based remote sensing for plant trait mapping. *Ecol. Complex.* 15, 1–16. <https://doi.org/10.1016/j.ecocom.2013.06.003>.
- Houghton, R.A., Hall, F., Goetz, S.J., 2009. Importance of biomass in the global carbon cycle. *J. Geophys. Res. Biogeosci.* 114 <https://doi.org/10.1029/2009JG000935>.
- Hovi, A., Raatio, P., Rautiainen, M., 2017. A spectral analysis of 25 boreal tree species. *Silva Fenn.* 51 <https://doi.org/10.14214/sf.7753>.
- Inamdar, D., Kalacska, M., Arroyo-Mora, J.P., Leblanc, G., 2021a. The directly-georeferenced hyperspectral point cloud: preserving the integrity of hyperspectral imaging data. *Front. Remote Sens.* 2, 9. <https://doi.org/10.3389/frsen.2021.675323>.
- Inamdar, D., Kalacska, M., Leblanc, G., Arroyo-Mora, J.P., 2021b. Implementation of the directly-georeferenced hyperspectral point cloud. *MethodsX* 8, 101429. <https://doi.org/10.1016/j.mex.2021.101429>.
- Jucker, T., Bongalov, B., Burslem, D.F.R.P., Nilus, R., Dalponte, M., Lewis, S.L., Phillips, O.L., Qie, L., Coomes, D.A., 2018. Topography shapes the structure, composition and function of tropical forest landscapes. *Ecol. Lett.* 21, 989–1000. <https://doi.org/10.1111/ele.12964>.
- Kembel, S.W., Ackerly, D.D., Blomberg, S.P., Cornwell, W.K., Cowan, P.D., Helmus, M.R., Morlon, H., Webb, C.O., 2020. picante: Integrating Phylogenies and Ecology.
- Kembel, S.W., Cowan, P.D., Helmus, M.R., Cornwell, W.K., Morlon, H., Ackerly, D.D., Blomberg, S.P., Webb, C.O., 2010. Picante: R tools for integrating phylogenies and ecology. *Bioinformatics* 26, 1463–1464. <https://doi.org/10.1093/bioinformatics/btp166>.
- Laliberté, E., 2018. Measuring specific leaf area and water content [WWW Document]. protocols.io. URL (accessed 2.2.22). <https://www.protocols.io/view/measuring-specific-leaf-area-and-water-content-p3tdqmn>.
- Laliberté, E., Legendre, P., 2010. A distance-based framework for measuring functional diversity from multiple traits. *Ecology* 91, 299–305. <https://doi.org/10.1890/08-2244.1>.
- Laliberté, E., Legendre, P., Shipley, B., 2014. FD: measuring functional diversity from multiple traits, and other tools for functional ecology. R Package Version 1, 0–12.
- Laliberté, E., Schweiger, A.K., Legendre, P., 2020. Partitioning plant spectral diversity into alpha and beta components. *Ecol. Lett.* 23, 370–380. <https://doi.org/10.1111/ele.13429>.
- Lambert, M.-C., Ung, C.-H., Raulier, F., 2005. Canadian national tree aboveground biomass equations. *Can. J. For. Res.* 35, 1996–2018. <https://doi.org/10.1139/x05-112>.
- Lamlom, S.H., Savidge, R.A., 2003. A reassessment of carbon content in wood: variation within and between 41 North American species. *Biomass Bioenergy* 25, 381–388. [https://doi.org/10.1016/S0961-9534\(03\)00033-3](https://doi.org/10.1016/S0961-9534(03)00033-3).
- Leboeuf, A., Pomerleau, I., Vézéau, S., Lacroix, S., 2015. Province-wide LiDAR Data acquisition: impact analysis and recommendations. *Ministère des Forêts, de la Faune et des Parcs (MFPP) du Québec*.
- Lehnert, L.W., Meyer, H., Obermeier, W.A., Silva, B., Regeling, B., Bendix, J., 2019. Hyperspectral data analysis in R: the hsdar package. *J. Stat. Softw.* 89, 1–23. <https://doi.org/10.18637/jss.v089.i12>.
- Leitão, P.J., Schwieder, M., Pedroni, F., Sanchez, M., Pinto, J.R.R., Maracahipes, L., Bustamante, M., Hostert, P., 2019. Mapping woody plant community turnover with space-borne hyperspectral data – a case study in the cerrado. *Remote Sens. Ecol. Conserv.* 5, 107–115. <https://doi.org/10.1002/rse.2.91>.

- Li, Y., Li, M., Li, C., Liu, Z., 2020. Forest aboveground biomass estimation using landsat 8 and sentinel-1A data with machine learning algorithms. *Sci. Rep.* 10, 9952. <https://doi.org/10.1038/s41598-020-67024-3>.
- Liu, X., Trogisch, S., He, J.-S., Niklaus, P.A., Bruelheide, H., Tang, Z., Erfmeier, A., Scherer-Lorenzen, M., Pietsch, K.A., Yang, B., Kühn, P., Schmid, B., Ma, K., 2018. Tree species richness increases ecosystem carbon storage in subtropical forests. *Proc. R. Soc. B Biol. Sci.* 285, 20181240. <https://doi.org/10.1098/rspb.2018.1240>.
- Lohmöller, J.-B., 2013. Latent Variable Path Modeling with Partial Least Squares, Softcover reprint of the original, 1st ed. 1989 Edition. ed. Physica, Heidelberg.
- Lopatin, J., Kattenborn, T., Galleguillos, M., Perez-Quezada, J.F., Schmidlein, S., 2019. Using aboveground vegetation attributes as proxies for mapping peatland belowground carbon stocks. *Remote Sens. Environ.* 231, 111217 <https://doi.org/10.1016/j.rse.2019.111217>.
- Meireles, J.E., Schweiger, A.K., Cavender-Bares, J.M., 2017. spectrolab: Class and Methods for Hyperspectral Data. R package version 0.0.2.
- Naik, P., Dalponte, M., Bruzzone, L., 2021. Prediction of Forest aboveground biomass using multitemporal multispectral remote sensing data. *Remote Sens.* 13, 1282. <https://doi.org/10.3390/rs13071282>.
- NRCan, 2008. Canada's National Forest Inventory ground sampling guidelines: specifications for ongoing measurement.
- Oksanen, J., Blanchet, F.G., Friendly, M., Kindt, R., Legendre, P., McGlinn, D., Minchin, P.R., O'Hara, R.B., Simpson, G.L., Solymos, P., Stevens, M.H.H., Szoecs, E., Wagner, H., 2020. vegan: Community Ecology Package.
- Ollinger, S.V., 2011. Sources of variability in canopy reflectance and the convergent properties of plants. *New Phytol.* 189, 375–394. <https://doi.org/10.1111/j.1469-8137.2010.03536.x>.
- Ollinger, S.V., Smith, M.-L., 2005. Net primary production and canopy nitrogen in a temperate Forest landscape: an analysis using imaging spectroscopy, modeling and field data. *Ecosystems* 8, 760–778. <https://doi.org/10.1007/s10021-005-0079-5>.
- Osei Darko, P., Kalacska, M., Arroyo-Mora, J.P., Fagan, M.E., 2021. Spectral complexity of hyperspectral images: a new approach for mangrove classification. *Remote Sens.* 13, 2604. <https://doi.org/10.3390/rs13132604>.
- Palmer, M.W., Earls, P.G., Hoagland, B.W., White, P.S., Wohlgemuth, T., 2002. Quantitative tools for perfecting species lists. *Environmetrics* 13, 121–137. <https://doi.org/10.1002/env.516>.
- Paquette, A., Messier, C., 2011. The effect of biodiversity on tree productivity: from temperate to boreal forests. *Glob. Ecol. Biogeogr.* 20, 170–180. <https://doi.org/10.1111/j.1466-8238.2010.00592.x>.
- Paradis, E., Schliep, K., 2019. ape 5.0: an environment for modern phylogenetics and evolutionary analyses. In: *R Bioinformatics*. Oxf. Engl. 35, pp. 526–528. <https://doi.org/10.1093/bioinformatics/bty633>.
- Parc national du Mont Mégantic (PNMM), 2007. Synthèse de connaissance, Parc national du Mont Mégantic. Société des Établissements de Plein air du Québec, Québec, QC, Canada.
- Pebesma, E., 2018. Simple features for R: standardized support for spatial vector data. *R J.* 10, 439. <https://doi.org/10.32614/RJ-2018-009>.
- Phiri, D., Simwanda, M., Salekin, S., Nyirenda, V.R., Murayama, Y., Ranagalage, M., 2020. Sentinel-2 data for land cover/use mapping: a review. *Remote Sens.* 12, 2291. <https://doi.org/10.3390/rs12142291>.
- Puliti, S., Hauglin, M., Breidenbach, J., Montesano, P., Neigh, C.S.R., Rahlf, J., Solberg, S., Klingenberg, T.F., Astrup, R., 2020. Modelling above-ground biomass stock over Norway using national forest inventory data with ArcticDEM and Sentinel-2 data. *Remote Sens. Environ.* 236, 111501 <https://doi.org/10.1016/j.rse.2019.111501>.
- Qian, H., Jin, Y., 2016. An updated megaphylogeny of plants, a tool for generating plant phylogenies and an analysis of phylogenetic community structure. *J. Plant Ecol.* 9, 233–239. <https://doi.org/10.1093/jpe/rtv047>.
- Rautiainen, M., Stenberg, P., Nilson, T., Kuusik, A., 2004. The effect of crown shape on the reflectance of coniferous stands. *Remote Sens. Environ.* 89, 41–52. <https://doi.org/10.1016/j.rse.2003.10.001>.
- Rawat, M., Arunachalam, K., Arunachalam, A., Alatalo, J., Pandey, R., 2019. Associations of plant functional diversity with carbon accumulation in a temperate forest ecosystem in the Indian Himalayas. *Ecol. Indic.* 98, 861–868. <https://doi.org/10.1016/j.ecolind.2018.12.005>.
- Reich, P.B., 2014. The world-wide 'fast-slow' plant economics spectrum: a traits manifesto. *J. Ecol.* 102, 275–301. <https://doi.org/10.1111/1365-2745.12211>.
- Reich, P.B., 2012. Key canopy traits drive forest productivity. *Proc. R. Soc. B Biol. Sci.* 279, 2128–2134. <https://doi.org/10.1098/rspb.2011.2270>.
- Reich, P.B., Walters, M.B., Ellsworth, D.S., 1997. From tropics to tundra: global convergence in plant functioning. *Proc. Natl. Acad. Sci.* 94, 13730–13734. <https://doi.org/10.1073/pnas.94.25.13730>.
- Rocchini, D., Luque, S., Pettorelli, N., Bastin, L., Doktor, D., Faedi, N., Feilhauer, H., Féret, J.-B., Foody, G.M., Gavish, Y., Godinho, S., Kunin, W.E., Lausch, A., Leitão, P., J., Marcantonio, M., Neteler, M., Ricotta, C., Schmidlein, S., Vihervaara, P., Wegmann, M., Nagendra, H., 2018. Measuring β-diversity by remote sensing: a challenge for biodiversity monitoring. *Methods Ecol. Evol.* 9, 1787–1798. <https://doi.org/10.1111/2041-210X.12941>.
- Ruiz-Benito, P., Gómez-Aparicio, L., Paquette, A., Messier, C., Kattge, J., Zavala, M.A., 2014. Diversity increases carbon storage and tree productivity in spanish forests. *Glob. Ecol. Biogeogr.* 23, 311–322. <https://doi.org/10.1111/geb.12126>.
- Schweiger, A.K., Cavender-Bares, J., Townsend, P.A., Hobble, S.E., Madritch, M.D., Wang, R., Tilman, D., Gamon, J.A., 2018. Plant spectral diversity integrates functional and phylogenetic components of biodiversity and predicts ecosystem function. *Nat. Ecol. Evol.* 2, 976–982. <https://doi.org/10.1038/s41559-018-0551-1>.
- Schweiger, A.K., Laliberté, E., 2022. Plant beta-diversity across biomes captured by imaging spectroscopy. *Nat. Commun.* 13, 2767. <https://doi.org/10.1038/s41467-022-30369-6>.
- Serbin, S.P., Townsend, P.A., 2020. Scaling functional traits from leaves to canopies. In: Cavender-Bares, J., Gamon, J.A., Townsend, P.A. (Eds.), *Remote Sensing of Plant Biodiversity*. Springer International Publishing, Cham, pp. 43–82. <https://doi.org/10.1007/978-3-030-33157-3>.
- Shmueli, G., Sarstedt, M., Hair, J.F., Cheah, J.-H., Ting, H., Vaithilingam, S., Ringle, C. M., 2019. Predictive model assessment in PLS-SEM: guidelines for using PLSpredict. *Eur. J. Mark.* 53, 2322–2347. <https://doi.org/10.1108/EJM-02-2019-0189>.
- Singh, A., Serbin, S.P., McNeil, B.E., Kingdon, C.C., Townsend, P.A., 2015. Imaging spectroscopy algorithms for mapping canopy foliar chemical and morphological traits and their uncertainties. *Ecol. Appl.* 25, 2180–2197. <https://doi.org/10.1890/14-2098.1>.
- Smith, M.-L., Ollinger, S., Martin, M., Aber, J., Hallett, R., Goodale, C., 2002. Direct estimation of aboveground forest productivity through hyperspectral remote sensing of canopy nitrogen. *Ecol. Appl.* 12, 1286–1302. <https://doi.org/10.12307/3099972>.
- Tenenhaus, M., Vinzi, V.E., Chatelin, Y.-M., Lauro, C., 2005. PLS path modeling. *Comput. Stat. Data anal.* 48, 159–205. <https://doi.org/10.1016/j.csda.2004.03.005>.
- Tilman, D., Lehman, C.L., Thomson, K.T., 1997. Plant diversity and ecosystem productivity: theoretical considerations. *Proc. Natl. Acad. Sci.* 94, 1857–1861. <https://doi.org/10.1073/pnas.94.5.1857>.
- Vellend, M., Béhé, M., Carteron, A., Crofts, A., Danneyrolles, V., Gamhewa, H., Ni, M., Rinas, C., Watts, D., 2021. Plant responses to climate change and an elevational gradient in mont Mégantic National Park, Québec, Canada. *Northeast. Nat.* 28. <https://doi.org/10.1656/045.028.s1102>.
- Violle, C., Navas, M.-L., Vile, D., Kazakou, E., Fortunel, C., Hummel, I., Garnier, E., 2007. Let the concept of trait be functional! *Oikos* 116, 882–892. <https://doi.org/10.1111/j.0030-1299.2007.15559.x>.
- Wallis, C.I.B., Brehm, G., Donoso, D.A., Fiedler, K., Homeier, J., Paulsch, D., Stübenbach, D., Tiede, Y., Brandl, R., Farwig, N., Bendix, J., 2017. Remote sensing improves prediction of tropical montane species diversity but performance differs among taxa. *Ecol. Indic.* 83, 538–549. <https://doi.org/10.1016/j.ecolind.2017.01.022>.
- Wallis, C.I.B., Homeier, J., Peña, J., Brandl, R., Farwig, N., Bendix, J., 2019. Modeling tropical montane forest biomass, productivity and canopy traits with multispectral remote sensing data. *Remote Sens. Environ.* 225, 77–92. <https://doi.org/10.1016/j.rse.2019.02.021>.
- Wang, R., Gamon, J., Cavender-Bares, J., Townsend, P., Zygielbaum, A., 2017. The spatial sensitivity of the spectral diversity-biodiversity relationship: an experimental test in a prairie grassland. *Ecol. Appl. Publ. Ecol. Soc. Am.* 28 <https://doi.org/10.1002/eap.1669>.
- Wang, R., Gamon, J.A., 2019. Remote sensing of terrestrial plant biodiversity. *Remote Sens. Environ.* 231, 111218 <https://doi.org/10.1016/j.rse.2019.111218>.
- Webb, C.O., Ackerly, S.D., Kembel, S.W., 2008. Phylocom: software for the analysis of phylogenetic community structure and trait evolution. *Bioinformatics* 24, 2098–2100. <https://doi.org/10.1093/bioinformatics/btn358>.
- Webb, C.O., Donoghue, M.J., 2005. Phyloomatic: tree assembly for applied phylogenetics. *Mol. Ecol. Notes* 5, 181–183. <https://doi.org/10.1111/j.1471-8286.2004.00829.x>.
- Williams, D.L., 1991. A comparison of spectral reflectance properties at the needle, branch, and canopy level for selected conifer species. *Remote Sens. Environ.* 35, 79–93. [https://doi.org/10.1016/0034-4257\(91\)90002-N](https://doi.org/10.1016/0034-4257(91)90002-N).
- Williams, L.J., Cavender-Bares, J., Townsend, P.A., Couture, J.J., Wang, Z., Stefanski, A., Messier, C., Reich, P.B., 2021. Remote spectral detection of biodiversity effects on forest biomass. *Nat. Ecol. Evol.* 5, 46–54. <https://doi.org/10.1038/s41559-020-01329-4>.
- Wright, I.J., Reich, P.B., Westoby, M., Ackerly, D.D., Baruch, Z., Bongers, F., Cavender-Bares, J., Chapin, T., Cornelissen, J.H.C., Diemer, M., Flexas, J., Garnier, E., Groom, P.K., Gulias, J., Hikosaka, K., Lamont, B.B., Lee, T., Lee, W., Lusk, C., Midgley, J.J., Navas, M.-L., Niinemets, Ü., Oleksyn, J., Osada, N., Poorter, H., Poot, P., Prior, L., Pyankov, V.I., Roumet, C., Thomas, S.C., Tjoelker, M.G., Veneklaas, E.J., Villar, R., 2004. The worldwide leaf economics spectrum. *Nature* 428, 821–827. <https://doi.org/10.1038/nature02403>.
- Wu, Z., Snyder, G., Vadnais, C., Arora, R., Babcock, M., Stensaas, G., Doucette, P., Newman, T., 2019. User needs for future landsat missions. *Remote Sens. Environ.* 231, 111214 <https://doi.org/10.1016/j.rse.2019.111214>.
- Xiao, J., Chevallier, F., Gomez, C., Guanter, L., Hicke, J.A., Huete, A.R., Ichii, K., Ni, W., Pang, Y., Rahman, A.F., Sun, G., Yuan, W., Zhang, L., Zhang, X., 2019. Remote sensing of the terrestrial carbon cycle: a review of advances over 50 years. *Remote Sens. Environ.* 233, 111383 <https://doi.org/10.1016/j.rse.2019.111383>.
- Xu, Y., Zhang, Y., Shi, M., Lu, Z., 2020. Environmental variation, functional diversity and identity predicting community biomass in an old-growth subtropical broad-leaved forest. *Glob. Ecol. Conserv.* 23, e01093 <https://doi.org/10.1016/j.gecco.2020.e01093>.
- Yuan, Z., Wang, S., Ali, A., Gazol, A., Ruiz-Benito, P., Wang, X., Lin, F., Ye, J., Hao, Z., Loreau, M., 2018. Aboveground carbon storage is driven by functional trait composition and stand structural attributes rather than biodiversity in temperate mixed forests recovering from disturbances. *Ann. For. Sci.* 75, 67. <https://doi.org/10.1007/s13595-018-0745-3>.
- Zhao, Y., Zeng, Y., Zheng, Z., Dong, W., Zhao, D., Wu, B., Zhao, Q., 2018. Forest species diversity mapping using airborne LiDAR and hyperspectral data in a subtropical forest in China. *Remote Sens. Environ.* 213, 104–114. <https://doi.org/10.1016/j.rse.2018.05.014>.